The Journal of Clinical Endocrinology & Metabolism, 2021, Vol. XX, No. XX, 1–27
doi:10.1210/clinem/dgab195
Clinical Research Article

Clinical Research Article

Progesterone Receptors Promote Quiescence and Ovarian Cancer Cell Phenotypes via DREAM in p53-Mutant Fallopian Tube Models

Laura J. Mauro,[1,2] Megan I. Seibel,[1] Caroline H. Diep,[1] Angela Spartz,[1] Carlos Perez Kerkvliet,[1] Hari Singhal,[3] Elizabeth M. Swisher,[4] Lauren E. Schwartz,[5] Ronny Drapkin,[6] Siddharth Saini,[7] Fatmata Sesay,[7] Larisa Litovchick,[7] and Carol A. Lange[1,8]

[1]University of Minnesota, Masonic Cancer Center, Minneapolis, MN 55455, USA; [2]University of Minnesota, Department of Animal Science, St. Paul, MN 55108, USA; [3]Northwestern University, Department of Surgery, Feinberg School of Medicine, Chicago, IL 60611, USA; [4]University of Washington Seattle, Dept Obstetrics & Gynecology, Division of Gynecologic Oncology, Seattle, WA 98109, USA [5]University of Pennsylvania, Dept of Pathology and Laboratory Medicine, Philadelphia, PA 19104, USA; [6]University of Pennsylvania, Penn Ovarian Cancer Research Center, Dept Obstetrics & Gynecology, Philadelphia, PA 19104, USA; [7]Virginia Commonwealth University, Massey Cancer Center, Dept. Internal Medicine, Division of Hematology, Oncology & Palliative Care, Richmond, VA 23298, USA; [8]University of Minnesota, Dept Medicine, Division of Hematology, Oncology & Transplantation, Minneapolis, MN 55455, USA

ORCiD numbers: 0000-0003-4372-8299 (L. J. Mauro); 0000-0003-2751-3976 (C. A. Lange).

Abbreviations: ATP, adenosine triphosphate; BrdU, bromodeoxyuridine; cAMP, cyclic adenosine monophosphate; ChIP, chromatin immunoprecipitation; DCC, dextran-coated charcoal; DMEM, Dulbecco's Modified Eagle Medium; DYRK, dual-specificity tyrosine-regulated protein kinase; E2, estradiol; EV, empty vector; FBS, fetal bovine serum; FT, fallopian tube; FTE, fallopian tube epithelia; hFTE, human fallopian tube epithelia; HGSC, high-grade serous ovarian cancer; IHC, immunohistochemistry; IRB, institutional review board; NT, nontargeting; OC, ovarian cancer; PBS, phosphate-buffered saline; PR, progesterone receptor; qPCR, quantitative polymerase chain reaction; RT-qPCR, quantitative reverse transcription–polymerase chain reaction; RU486, mifepristone; SAβ-Gal, senescence-associated β-galactosidase; SDS-PAGE, sodium dodecyl sulfate–polyacrylamide gel electrophoresis; shRNA, short hairpin RNA; STIC, serous tubal intraepithelial carcinoma; STIL, serous tubal intraepithelial lesion.

Received: 30 October 2020; Editorial Decision: 19 March 2021; First Published Online: 23 March 2021; Corrected and Typeset: 25 May 2021.

Abstract

Context: The ability of ovarian steroids to modify ovarian cancer (OC) risk remains controversial. Progesterone is considered to be protective; recent studies indicate no effect or enhanced OC risk. Knowledge of progesterone receptor (PR) signaling during altered physiology that typifies OC development is limited.

Objective: This study defines PR-driven oncogenic signaling mechanisms in p53-mutant human fallopian tube epithelia (hFTE), a precursor of the most aggressive OC subtype.

ISSN Print 0021-972X ISSN Online 1945-7197
Printed in USA

Methods: PR expression in clinical samples of serous tubal intraepithelial carcinoma (STIC) lesions and high-grade serous OC (HGSC) tumors was analyzed. Novel PR-A and PR-B isoform-expressing hFTE models were characterized for gene expression and cell cycle progression, emboli formation, and invasion. PR regulation of the DREAM quiescence complex and DYRK1 kinases was established.

Results: STICs and HGSC express abundant activated phospho-PR. Progestin promoted reversible hFTE cell cycle arrest, spheroid formation, and invasion. RNAseq/biochemical studies revealed potent ligand-independent/-dependent PR actions, progestin-induced regulation of the DREAM quiescence complex, and cell cycle target genes through enhanced complex formation and chromatin recruitment. Disruption of DREAM/DYRK1s by pharmacological inhibition, HPV E6/E7 expression, or DYRK1A/B depletion blocked progestin-induced cell arrest and attenuated PR-driven gene expression and associated OC phenotypes.

Conclusion: Activated PRs support quiescence and pro-survival/pro-dissemination cell behaviors that may contribute to early HGSC progression. Our data support an alternative perspective on the tenet that progesterone always confers protection against OC. STICs can reside undetected for decades prior to invasive disease; our studies reveal clinical opportunities to prevent the ultimate development of HGSC by targeting PRs, DREAM, and/or DYRKs.

Key Words: progesterone, fallopian tube epithelia, DREAM, ovarian cancer, STIC, DYRK1 kinases

Ovarian cancer (OC) only accounts for about 3% of all cancers diagnosed in women in the United States, yet it is the most lethal of all gynecologic cancers and is the fifth leading cause of cancer deaths (1). Epidemiological studies have implicated reproductive status and hormone exposure in the pathogenesis of this disease (2). Parity, breastfeeding, and the use of oral contraceptives or hormone replacement therapy have been examined as either risk-inducing or preventive factors (3, 4). Progesterone, in particular, is theorized to be the protective steroid in these cases, presumably due to elevated endogenous progesterone during pregnancy or exposure to the synthetic progestin components of oral contraceptives. Full-term pregnancies, for example, are associated with reduced risk, with the greatest reduction observed for the less aggressive, low-grade type I tumors (5). The current or recent use of contemporary combined hormonal contraceptives (eg, lower estrogen dose, newer progestin compounds) resulted in a reduced risk of any OC subtype, in particular, endometrioid, mucinous, and serous (4). Yet, other studies have found that the use of oral and nonoral progestin-only contraceptives (eg, norethisterone, levonorgestrel, desogestrel, medroxyprogesterone acetate) did not diminish risk (4), and that estrogen-only and estrogen-progestin combination hormone replacement therapy use by postmenopausal women may actually increase ovarian cancer risk (6, 7). Therefore, the ability of ovarian steroids such as progesterone or estrogens to modify OC risk still remains highly controversial and the potential mechanisms involved are poorly understood.

The most common and aggressive OC subtype, high-grade serous ovarian cancer (HGSC), expresses abundant estrogen receptors (ER; 76% (8);) and progesterone receptors (PR; 35%) and ex vivo explants of these tumors exhibit functional PR signaling (8-10). It is believed that HGSC, in contrast to other subtypes, originates predominantly within the distal fimbriae of the fallopian tube (FT). The FT secretory epithelia acquire DNA damage and *TP53* mutations, forming early neoplasms known as serous tubal intraepithelial carcinomas (STICs) (11, 12). Recent evidence suggests that these lesions may be present for many years as "dormant" STICs (ie, serous tubal intraepithelial lesions—STIL) before progressing to an "active" STIC (12, 13). These "dormant" lesions possess TP53 mutations but often show little to no proliferative activity, similar to normal fallopian tube epithelia (FTE) (14). The evolution of these lesions to an "active" STIC is marked by enhanced proliferative capacity and the acquisition of additional genetic alterations that set the stage for seeding of metastases on the ovary and other organs and surfaces within the abdominal cavity. If such lesions also possess functional PR signaling, how this signaling differs from normal FTE and whether progestins modulate the survival and dissemination of these neoplasms is not known.

Signaling via nuclear PRs is mediated primarily by 2 distinct, co-expressed PR isoforms: the full-length PR-B (1-933

amino acids) and the N-terminally truncated PR-A (165-933 amino acids) (15). The ratio of PR isoforms in a cell, the presence of potential ligands and the posttranslational receptor modifications (ie, phosphorylation, sumoylation) all contribute to the downstream cellular outcomes of PR signaling (15-17). For example, phosphorylation of critical residues in these isoforms, such as Ser294, leads to unique Lys388 desumoylated PR species which drive distinct transcriptomes of phospho-PR target genes (18, 19). It is important to note that PR can sense input from steroid hormone signals, as well as multiple growth factor–initiated kinase pathways (16, 20). As such, signaling via these PR isoforms can occur in the absence (ie, ligand-independent) and presence (ie, ligand-dependent) of hormone; therefore, both states are critical to the functions of PR and many other steroid receptors (21, 22).

The biological effects of PR signaling are intimately connected to cell fate in normal and cancerous breast and uterine epithelia. In these tissues, PR is known to be tightly coupled to many cell cycle mediators, regulating cell cycle progression (23). It is accepted that progesterone signaling modulates fallopian tube epithelia (FTE) functions which support gamete and zygote transport and survival (24). Less well-studied are the progestins' effects on FTE cell fate. Immunohistochemical analyses and gene expression profiling of 3-dimensional primary FTE cultures suggests that these epithelia are quiescent, especially those in the early/mid luteal phase of the menstrual cycle when PR signaling is most prominent (25, 26). Yet, the molecular mechanisms involved in such progestin-induced regulation are poorly understood, most likely because development of in vitro PR-expressing FTE models has been difficult—loss of steroid receptor expression is common during the immortalization process.

For all cells, including FTE, the entry into G0 arrest or quiescence is thought to be associated with the active transcriptional repression of cell cycle dependent genes by the multimeric complex known as DREAM which consists of the DREAM-specific proteins, **D**imerization partner DP1/2, **R**b-like p130/p107, **E**2F4/5 plus the core complex **M**uvB (LIN9, LIN37, LIN52, LIN54, RBBP4 proteins (27)). Such quiescence or dormancy is a natural state of certain cell types, especially stem cell progenitors, and has recently been recognized as a common feature of many cancers. Cycling between dormancy and proliferation may be essential for the acquisition of new mutations, survival in a suboptimal environment, metastasis, and chemoresistance (28, 29). Interestingly, malignant OC tumor cells in multicellular aggregates, as observed in ascites, appear to be in a dormant state (30). Amplifications, copy number losses, or gains in genes encoding subunits of the MuvB complex are commonly present in HGSC tumors and can be associated with poor prognosis (27, 31). These studies highlight the importance of understanding how cells enter/exit quiescence in HGSC progression. However, the mechanisms regulating DREAM and cell cycle progression have not been evaluated in normal fallopian tube epithelia or in p53-mutant models of early disease.

Our studies described here reveal that nuclear and focal activated PR is robustly expressed in STIC lesions and invasive HGSC. Using novel PR-expressing human fallopian tube epithelial (hFTE) cell models, we show that progestins are able to promote cellular phenotypes that could support STIC lesion shedding and dissemination, including cell-cell aggregation/spheroid formation and collagen invasion. In the absence of progestins, PR-A isoforms act as dominant inhibitors of DREAM, promoting permissive cell cycle progression and migration, while both liganded receptor isoforms associate with and activate DREAM as well as dual-specificity tyrosine-regulated protein kinases (DYRKs), driving cells into a quiescent state that may support early ovarian cancer progression.

Methods

General Reagents

R5020 (Perkin Elmer), progesterone (P4; Sigma-Aldrich), estradiol (E2; Sigma-Aldrich), mifepristone (RU486, Sigma-Aldrich), and onapristone (Context Therapeutics) stocks were prepared in ethanol (EtOH). Harmine (Sigma-Aldrich) stock was prepared in dimethyl sulfoxide. Epidermal growth factor (EGF; Sigma-Aldrich) was prepared in 10 mM acetic acid with 0.1% bovine serum albumin (BSA).

Human Tissues

Fresh frozen normal fallopian tube (FT) tissues were acquired from patients undergoing salpingo-oophorectomy or total abdominal hysterectomy with bilateral salpingo-oophorectomy at the Fairview-University of Minnesota Hospital. Biospecimen procurement protocols were approved as institutional review board (IRB)-exempt and administered through the Clinical and Translational Sciences Institute's Biorepository & Laboratory Services BioNet division. FT tissue was dissected from surrounding tissues, snap-frozen on dry ice and stored at −80 °C until analysis.

Cases used for immunohistochemistry analyses were selected from University of Pennsylvania Medicine patients who were diagnosed with high-grade serous ovarian cancer (HGSC) and showed evidence of serous tubal intraepithelial carcinoma (STIC) lesions within the FT. Most of these cases also exhibited invasive HGSC within FT stroma and/or

associated ovarian tissues; both STIC and HGSC sections were available for analysis. Procurement of biospecimens was covered by Penn Ovarian Cancer Research Center Biotrust Collection IRB protocol #702679. De-identified formalin-fixed paraffin-embedded blocks were obtained and sections cut and processed as outlined below.

Fresh normal FT tissue utilized for the establishment of the original UWFT.1681 cell line was collected from a University of Washington Seattle Medicine patient undergoing salpingo-oophorectomy. This patient provided informed consent under a protocol approved by the IRB of the University of Washington (#2872).

Immunohistochemistry

Four-micron thick sections of formalin-fixed tissue were used for immunoperoxidase analysis after baking at 60 °C for 1 hour, followed by deparaffinization and rehydration in successive xylene, ethanol, and water washes. The sections were blocked with 3% hydrogen peroxide in methanol and antigen retrieval was performed in a pressure incubator (Biocare Medical) at 123 °C in citrate buffer (DAKO Target Retrieval Solution). Slides were cooled and transferred to Tris-buffered saline. Primary antibodies and conditions are listed in Supplemental Table 1 (32). The secondary antibody was used per protocols and reagents in the DAKO Envision + System. The sections were developed using 3,3′-diaminobenzidine (DAB; Sigma Chemical Company) as substrate and counter-stained with Mayer's Hematoxylin. Bright-field images were acquired in a Huron Tissuescope LE equipped with a Nikon Plan Apo 20X Objective Lens NA 0.75 housed and managed by the University of Minnesota University Imaging Centers. Scans were subsequently analyzed, and images captured and calibrated in Huron Viewer software (Huron Digital Pathology). Identity of STICs was verified by presence of atypical histology and scoring for presumed p53 mutations, including p53 missense mutation characterized by strong staining, null p53 mutation with little to no staining, or wild-type p53 with blush staining (33). PR and p-PR staining was scored as nondetectable/low intensity (–/+) to high intensity (+++) relative to the analyzed tissues. Relative intensity of p-PR staining is illustrated in Supplemental Figure 1 (32). Case information, mutations, and staining intensity are summarized in Fig. 1C.

Cell Lines and Culturing

All cell lines were maintained at 37 °C under 5% CO_2 in water-jacketed incubators. FT282 cells were cultured in Dulbecco's Modified Eagle Medium (DMEM)/F12 (Corning) supplemented with 10% charcoal stripped fetal bovine serum (DCC, Hyclone) and 1% penicillin-streptomycin (Gibco). Murine oviductal epithelium (MOE (34)) cells were gifted from Dr. Joanna Burdette (University of Illinois at Chicago) and were cultured in Minimum Essential Medium-Alpha (Corning) supplemented with 10% fetal bovine serum (FBS, Corning), 1% penicillin-streptomycin (Gibco), 1.1 µg/mL gentamicin (Abcam), 1.1% ITS (Corning), 2 ng/mL epidermal growth factor (Sigma-Aldrich), 20 ng/mL estradiol (Sigma-Aldrich) and 1% L-glutamine (Gibco). UWFT.1681 cells were cultured in MEGM (Lonza) supplemented with MEGM SingleQuots supplements (Lonza), 1% FBS, and 1% penicillin-streptomycin. All cell lines were routinely tested for mycoplasma using an e-Myco Plus Mycoplasma PCR Detection kit (Bulldog Bio Inc) and confirmed to be negative prior to experimentation.

Stable Cell Line Generation

Stable hFTE PR-expressing lines were generated by transducing FT282 cells with pLenti-CMV neo lentiviral vector containing PR-A or PR-B. Stable pools were selected and maintained in 0.2 mg/mL G418 (Corning) and then plated as single cells to generate empty vector (EV), PR-A, and PR-B clonal lines. Stable shDYRK1A (clones TRCN0000000523 and 524) expressing cell lines and shDYRK1B (clones TRCN0000002140 and 2141) expressing cell lines were generated by transducing FT282 PR-B+ and PR-A+ cells with pLKO.1 lentiviral vector containing target gene short hairpin RNA (shRNA) sequences for DYRK1A (AATACAAGAATCAACTGCTGG and AAAGTCCAAGGTATTAGCAGC) or DYRK1B (TAGCAGCAATTCCAGTCAAGG and ATATAGTACTTCATCTCCGTG). Stable pools were selected and maintained in 1 µg/mL puromycin and 0.2 mg/mL G418. Original UWFT.1681 cell line was established using dispersed FT epithelia from fresh primary FT tissues. Cells were immediately plated on 100 mm plates in MEGM media (Lonza) with 1% FBS. After 24-hour culturing with fibroblast adherence, supernatant was transferred serially to new plates for FTE cultures. Epithelial purity was confirmed by immunohistochemical evaluation of cytokeratins using the AE1/AE3 antibodies. Confluent FTE were infected with HPV E6/E7 as previously described (35).

Immunoblotting

Snap-frozen FT tissues were homogenized with a metal tissue pulverizer over dry ice. Protein was isolated with RIPA-lite lysis buffer (0.15 M NaCl, 6 mM Na_2HPO_4, 4 mM NaH_2PO_4, 2 mM EDTA, 0.1 M NaF, and 1% Triton-X 100 in H_2O supplemented with 1× complete mini protease

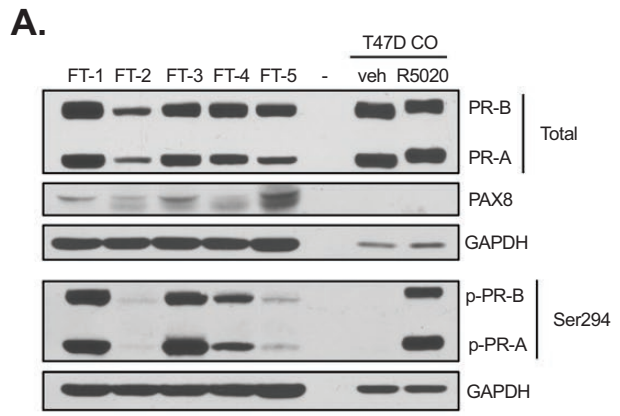

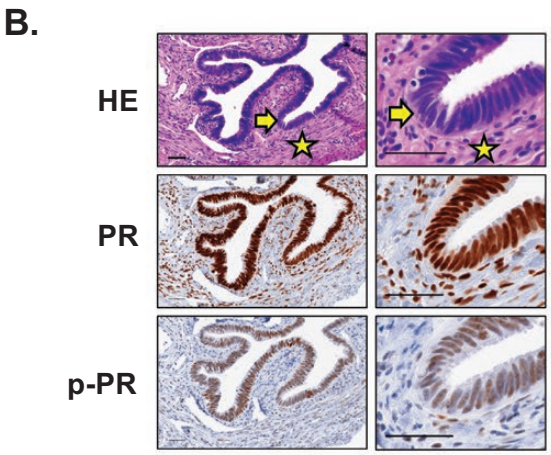

C.

		STAINING INTENSITY		
CASE	AGE	PR	p-PR	p-PR foci
1	74	+++	+++	x
2	70	-	+	
3	73	-/+	+	x
4	62	-/+	+	x
5	52	-/+	++	x
6	59	++	+	
7	55	-/+	+	x
8	65	++	++	x

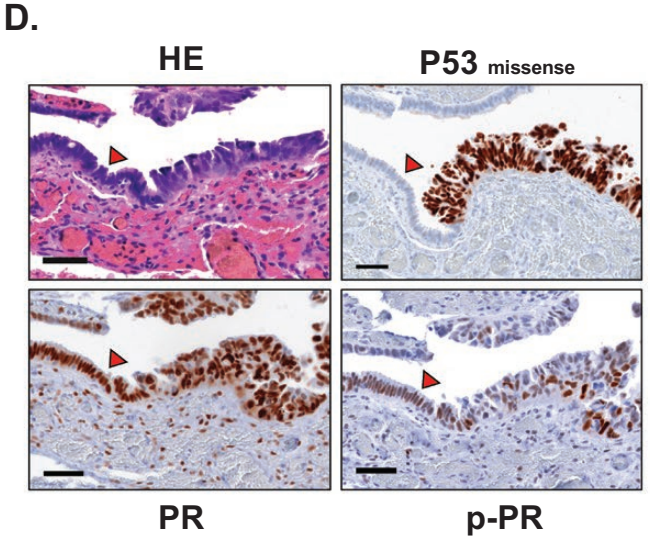

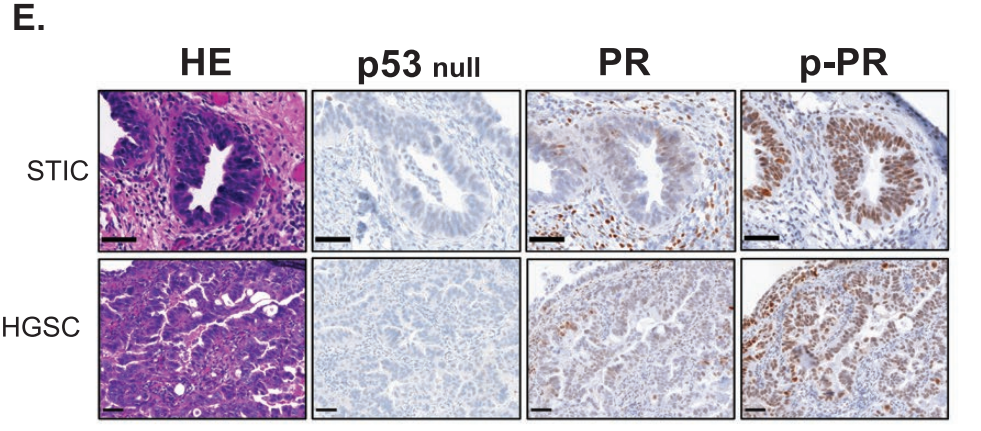

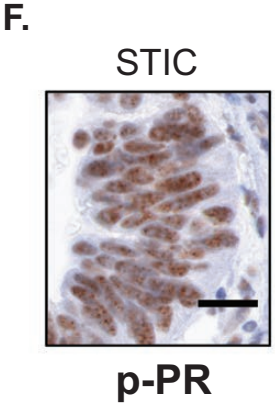

Figure 1. Progesterone receptor expression in normal human fallopian tube, STIC lesions, and invasive HGSC. **A,** Western blot analysis of PR-A and PR-B isoform expression and phosphorylated PR at Ser294 (p-PR-A, p-PR-B) expression in normal FT tissues. T47D CO line treated with vehicle (veh) or R5020 (10nM) for 1 hour as a positive control. PAX8 as FT positive control and GAPDH as loading control. **B,** Immunohistochemical (IHC) staining of normal FT tissues. Low (left) and high (right) magnification of hematoxylin-eosin (HE), PR and phosphoS294 PR (p-PR). Arrow indicates FT epithelia layer and star indicates FT stroma. Scale bars = 50 μm. **C,** Patient case information and IHC staining scores. Fallopian tube tissues obtained from patients with a HGSC diagnosis and presence of STIC lesions. Scoring of PR and p-PR proteins is indicated ranging from absence (–), light variable (–/+), low (+) to high (+++) intensity staining, based on relative intensity compared across the 8 cases. Presence of nuclear foci of p-PR staining within STICs is noted. **D,** IHC of representative STIC (case 1) exhibiting p53 missense mutation. Red arrowheads indicate normal hFTE. Scale bars = 50 μm. **E,** STIC and invasive HGSC (case 5). Scale bars = 50 μm. **F,** Nuclear foci of p-PR protein within STIC (case 1). Scale bars = 25 μm.

inhibitors [Roche], 1× PhosSTOP tablet [Roche], 25 mM β-glycerophosphate [BGP], 1 mM phenylmethanesulfonyl fluoride [PMSF], 20 µg/mL aprotinin [Fisher Bioreagents], 5 mM NaF, and 0.05 mM Na_3VO_4). Alternatively, adherent cells were washed with phosphate-buffered saline (PBS) and harvested with RIPA-lite lysis buffer. Lysates were cleared by centrifugation, quantified through Bradford assays using Bio-Rad reagent and equal protein concentrations were resolved on 8% sodium dodecyl sulfate–polyacrylamide gel electrophoresis (SDS-PAGE) gels. Proteins were then transferred to Immobilon-P polyvinylidene difluoride membranes (Millipore), probed with antibodies as listed in Supplemental Table 1 (32) and developed using SuperSignal West Pico Plus Chemiluminescent Substrate (Pierce).

Quantitative Reverse Transcription Polymerase Chain Reaction

Cells were plated in triplicate in phenol red–free DMEM/F12 supplemented with 5% DCC and treated the following day with vehicle or R5020 (10 nM). After the indicated time point, cells were washed with PBS and total RNA was harvested using TriPure Isolation Reagent (Roche) and isopropanol precipitation. According to the manufacturer's instructions, 1 µg of RNA was then reverse transcribed to cDNA using qScript cDNA SuperMix (Quanta Biosciences). The quantitative polymerase chain reaction (qPCR) was performed using FastStart Essential DNA SYBR Green Master (Roche) on a LightCycler 96 Real-Time PCR Instrument (Roche). Human primer sequences are listed in Supplemental Table 2 (32). The qPCR cycling conditions were as follows: initial denaturation at 95 °C (10 minutes), denature at 95 °C (10 seconds), anneal at 60 °C (10 seconds) and extension at 72 °C (5 seconds) for 45 cycles. Target gene expression levels were normalized to the TATA-box binding protein gene (TBP).

Cell Proliferation Assays

Screening of the proliferative capacity of EV and PR-expressing clonal lines was initially determined using the CellTiter-Glo assay (Promega). Cells were seeded in triplicate in opaque-walled 96 well plates in phenol-free DMEM/F12 supplemented with 10% DCC. After the cells were settled, a baseline Day 0 adenosine triphosphate (ATP) concentration was determined using the CellTiter-Glo 2.0 Assay (Promega) according to the manufacturer's instructions. Luminescence was measured using Synergy 2 (Biotek) and ATP concentrations were determined by generating an ATP standard curve with ATP disodium salt (Sigma). This process was repeated for the Day 2, 4, and 6 plates and the ATP concentrations were normalized by subtracting the Day 0 ATP concentration.

Immunofluorescence Assays

Cells were seeded on coverslips in phenol red–free DMEM/F12 supplemented with 5% DCC and treated the following day with vehicle or R5020 (10 nM). After 72 hours, cells were fixed with 4% paraformaldehyde and permeabilized with 0.1% Triton-X-100. All antibodies and blocking conditions are listed in Supplemental Table 1 (32). Coverslips were then mounted with ProLong Gold Antifade with DAPI (Molecular Probes) and analyzed using a Leica DM40000 B microscope. For quantitation of Ki67 staining, the percentages of Ki67+ cells were analyzed and calculated for ~10 fields per coverslip using a Leica DM40000 B microscope.

Senescence-Associated β-Galactosidase Activity Assays

Cells were seeded on coverslips in phenol red–free DMEM/F12 supplemented with 5% DCC and treated the following day with vehicle or R5020 (10 nM). After 72 hours, cells were washed with PBS, fixed with 4% paraformaldehyde, and stained for senescence-associated β-galactosidase (SAβ-Gal) activity using the Senescence β-Galactosidase Staining Kit (Cell Signaling Technology) according to the manufacturer's instructions. Cells were analyzed using a Leica DM40000 B microscope. The percentages of β-galactosidase+ cells were analyzed and averaged for ~10 fields per coverslip using a Leica DM40000 B microscope.

5-Bromo-2′-Deoxy-Uridine Immunofluorescence Assays

Cells were seeded on coverslips in phenol red–free DMEM/F12 supplemented with 5% DCC and treated the following day with vehicle or R5020 (10 nM). After 72 hours, cells were incubated with bromodeoxyuridine (BrdU), fixed with ethanol at –20 °C and stained for BrdU using the 5-Bromo-2′-deoxy-uridine Labeling and Detection Kit I (Sigma-Aldrich) according to the manufacturer's instructions. Percentages of BrdU+ cells were analyzed and averaged for ~10 fields per coverslip using a Leica DM40000 B microscope.

Migration Assays

Cells were harvested with 0.25% trypsin-EDTA (Invitrogen), washed and resuspended in phenol red–free DMEM/F12, and seeded in triplicate in 8-µm pore 24-well Transwell inserts (Corning). Medium (10% FBS or serum-free control medium) was placed in the bottom chamber of the 24-well plates and the cells were incubated for 18 hours. Membranes were then fixed with 4% paraformaldehyde,

cut out of the chamber and mounted with ProLong Gold Antifade with DAPI (Molecular Probes) and analyzed using a Leica DM40000 B microscope. The numbers of migrated cells were counted for 6 representative fields per chamber and averaged between conditions.

3D Spheroid Culture Assays

Cells were harvested with 0.25% trypsin-EDTA, washed, and resuspended in phenol red–free DMEM/F12 supplemented with 10% DCC. The cells were then sieved through 40-µm pore cell strainers (Falcon) and 8 single-cell suspensions (~1000 cells/well) were seeded per condition in 96-well U-bottom plates coated with 6 mg/mL poly(2-hydroxyethyl methacrylate) (Sigma). After 72 hours, single spheroids were imaged and measured on a Nikon Eclipse Ts3 microscope. Spheroid diameter was quantified for approximately 8 wells/data point.

3D Spheroid Invasion Assays

Collagen Type I (Corning) was neutralized to a pH of 7.4 and diluted to 2 mg/mL with phenol red–free DMEM/F12 supplemented with 10% DCC. Then 50 µL of diluted collagen was transferred into the wells of 96-well plates and incubated for 30 minutes at 37 °C to solidify the collagen. Using cold-cut pipette tips, single spheroids were individually harvested, resuspended in 100 µL collagen, and transferred on top of the solidified collagen layers. The spheroid-collagen layer was incubated for 1 hour at 37 °C to solidify before spheroid culture medium containing experimental treatments was plated on top. Spheroids were initially imaged using a Nikon Eclipse Ts3 microscope at Day 0 and then allowed to invade for 72 hours. Each spheroid was again imaged at the end of this 72-hour incubation. Areas (μm^2) for each spheroid at Day 0 and Day 3 were calculated from these digital images using ImageJ. The area of collagen invaded was calculated by subtracting the initial area of that spheroid at Day 0 from the final Day 3 area of that same spheroid to determine the relative invasion area for that single spheroid/well. Invasion area was quantified for approximately 6 to 8 wells per average data point.

Gene Expression Profiling

For RNAseq studies, clonal lines were pooled (EV #3,11; PR-A #7, 9; PR-B # 20, 24) and plated in triplicate. RNA was isolated using RNAeasy kit (Qiagen) according to the manufacturer's instructions. RNA quantity, quality, and size were determined by RiboGreen and Agilient BioAnalyzer. Strand-specific RNAseq libraries were created (Illumina TruSeq), quality/quantity verified (BioAnalyzer) followed by ~20 million 50 paired-end sequencing reads performed per library (HiSeq 2500 high-output mode) at the University of Minnesota Genomics Center. Bioinformatics analyses of RNAseq results was provided by Artificial Intelligene (Intelligene Technologies, Kenosha, WI; www.artificialintelligene.com). Briefly, each sample was aligned, BAM files sorted/indexed, and transcript abundance files created. Reads were aligned to the hg19 human genome using STAR (36). Cufflinks software (version 2.2.1) was used to generate transcript assemblies (37). Identification of differentially expressed genes using the reference and experimental groups of interest was performed using DESeq2 with a cutoff of ≥ 2-fold (38). Cluster analyses on sample groups was calculated where union of all the genes and their expression fragments per kilobase of exon per million reads (FPKM) values within that group were generated to build a read count matrix for the groups of interest. Unsupervised and other machine learning techniques were applied to this composite read count matrix of interest. R packages, including ggplot2, heatmap.2, and Pheatmap, were used to build various heatmaps with sample-feature heatmaps representing the signal intensity of a feature for any given sample. The volcano plots were created using data from differential expression values downloaded from the Artificial Intelligene interface and then R software (v 3.5.2) was implemented for the creation of these plots. Functional pathway enrichment in the gene list of interest was performed using gene set enrichment analyses (39) on Gene Ontology, Broad Institute, and Reactome input datasets from Artificial Intelligene (40). RNAseq data is available through the Gene Expression Omnibus (GEO) database (41).

Immunoprecipitations

Cells were seeded in phenol red–free DMEM/F12 supplemented with 5% DCC and treated the following day with vehicle or R5020 (10 nM). After the indicated time point, cells were washed with PBS and harvested with PBS supplemented with Protease-inhibitor Cocktail Set 1 (Calbiochem, 1:100) and Protease-inhibitor Cocktail Set 2 (Calbiochem, 1:500). Cells were pelleted through centrifugation and snap-frozen on dry ice. For immunoprecipitations, cell pellets were lysed in EBC buffer (Boston Bioproducts) supplemented with Protease-inhibitor Cocktail Set 1 (1:100), Protease-inhibitor Cocktail Set 2 (1:500) and 2-mercaptoethanol (1:10000). To immunoprecipitate DREAM and B-MYB/MMB complexes, 2 mg of lysate were incubated with 1 µg LIN37 antibody (Bethyl) and protein A sepharose

CL-4B beads (GE Healthcare) overnight at 4 °C. The samples were then washed with EBC, eluted with SDS-PAGE gel loading buffer and resolved on SDS-PAGE gels using standard protocols. After transfer to nitrocellulose membrane (Bio-Rad), the proteins of interest were probed with antibodies listed in Supplemental Table 1 (32) and protein band densities were calculated using ImageJ software as previously described (31).

Flow Cytometry

Cells were seeded in phenol red–free DMEM/F12 supplemented with 5% DCC and treated the following day with vehicle or R5020 (10 nM). After 24 hours, cells were collected, fixed, and stained as described (42). Cells were stained with Hoechst 33342 DNA-specific dye (Invitrogen). Acquisition and separation of the phases of the cell cycle were performed on a BD LSRFortessa Flow Cytometer System (BD Biosciences). Data analysis was performed using FlowJo v10 software (BD Biosciences).

Chromatin Immunoprecipitation

Cells were seeded in phenol-free DMEM/F12 supplemented with 5% DCC and treated the following day with vehicle or R5020 (10 nM) for 3 hours. Cells were then fixed, harvested, and lysed according to optimized manufacturer's instructions using the ChIP-IT Express Magnetic Chromatin Immunoprecipitation Kit (Active Motif). Samples were homogenized using a Bioruptor sonicator (Diagenode, Inc.). Chromatin immunoprecipitation (ChIP) reactions were incubated overnight on an end-to-end rotator using antibodies listed in Supplemental Table 1 (32). Samples were washed, eluted, reverse cross-linked, and treated with Proteinase K according to manufacturer's instructions (Active Motif). DNA was analyzed by reverse transcriptase–qPCR (RT-qPCR) using primers and chromosomal coordinates listed in Supplemental Table 3 (32).

Statistical Analyses

For all datasets, a Shapiro-Wilk normality test for normal distribution was performed followed by, as appropriate, a 1-way or 2-way analysis of variance (ANOVA) in combination with the Tukey multiple comparisons (Prism 8; GraphPad software). Statistical significance was set at $P < 0.05$ and graphs of continuous variable data show the mean ± standard deviation (n = sample size). All data presented is representative of at least 3 independent replicate experiments.

Results

Progesterone Receptor Expression in Normal Fallopian Tube, STIC Lesions, and Invasive HGSC

Little is known about PR or the PR phosphospecies expressed in normal fallopian tube (FT) epithelia or in neoplasms of these cells. Therefore, we examined the expression of both PR and phospho-Ser294 PR in normal FT and STIC lesions. Immunodetection of phospho-S294 PR was performed using a custom polyclonal antibody developed in our laboratory and previously validated for cellular protein assays and immunohistochemistry (IHC) of breast cancer tissue microarrays (19). Detection of "total" PR (ie, the combination of both unphosphorylated and multiple phosphospecies of both isoforms) was conducted with a commercial monoclonal antibody routinely used by our lab (SCBT sc-166169; Supplemental Table 1 (32)) as well as a clinical monoclonal antibody (Dako 3569 cl PgR636; Supplemental Table 1) (32). Western blot analyses of normal human FT tissues confirmed robust expression of both total PR-A and PR-B isoforms in all samples, as well as strong (3/5 cases) to weak (2/5 cases) expression of phosphorylated PR protein at Ser294 (p-S294, p-PR; Fig. 1A). This expression is localized primarily to the epithelial layer lining the FT, with nuclear staining of both PR isoforms and the phosphorylated S294 proteins of both isoforms (Fig. 1B).

We first reported that ~35% of metastatic HGSC tumors express abundant progesterone receptors (8). Herein, FT and associated HGSC tumor tissues from each HGSC patients with confirmed STIC lesions and invasive HGSC were stained for p53, total PR, and p-PR expression (Fig. 1C-1F; Supplemental Fig. 1 (32)). Both PR and p-PR staining was observed in STICs (Fig. 1C-1D) and this expression was retained in invasive HGSC tissue when present, whether localized within the FT stroma or ovarian tissue (Fig. 1E). Interestingly, p-PR staining was often localized within punctate nuclear foci (Fig. 1F); a phenotype indicative of active transcriptional complexes (43, 44). Such nuclear foci were more commonly observed in STIC lesions but were occasionally seen in adjacent normal FTE. As expected, the presence or intensity of the total vs phosphorylated PR protein was sometimes discordant; p-PR protein was consistently present when total PR was sometimes low or nondetectable in the same tissue. Additional staining with a diagnostic PR monoclonal antibody revealed the same staining patterns (Dako 3569 cl PgR636; data not shown). We have reported differential detection of total PR and phospho-PR proteins in breast cancer tissues using similar antibodies and antibody protocols (19, 32). This may be due to the inherent differences in the recognition

of multiple epitopes by polyclonal antisera versus single epitope recognition by a monoclonal antibody, as well as the potential for epitope masking due to phosphorylation or other posttranslational modifications of PRs present in multiprotein nuclear complexes. In addition, we and others have reported differing turnover rates of PR isoforms relative to their PR phosphospecies (45, 46).

Overall, these IHC analyses demonstrate that activated progesterone receptor species (ie, phospho-S294 PR) can be reliably detected and are well-expressed in STICs as well as in HGSC tumors localized to the fallopian tube and the ovary.

Generation of PR-Expressing Human Fallopian Tube Epithelial Models

The lack of robust cell models of human FT epithelia that express ovarian steroid receptors, such as PRs, has hampered mechanistic studies of steroid receptor signaling. Immortalization procedures and 2-dimensional culturing invariably leads to loss of endogenous receptor expression. To facilitate our studies, the FT secretory cell line which stably expresses the p53 missense mutation R175H (47), was genetically engineered to express either the PR-A or PR-B isoform. Multiple clones of empty vector controls (EV; #3,11), PR-A+ (#7, 8, 9) and PR-B+ (#15, 20, 24) cells were isolated, which showed similar protein expression to T47D CO breast carcinoma cells expressing endogenous PRs (Fig. 2A). Only the PR+ clones exhibited rapid activation of PR isoforms with phosphorylation of the Ser294 site following treatment with R5020, a stable progestin that binds specifically to PR (Figs. 2B-2C). As expected, this potent PR agonist shows activation of phosphorylation at concentrations between 1 nM and 10 µM whereas the natural ligand, progesterone, shows activation at a slightly narrower concentration range of 10 nM to 10 µM (Supplemental Fig. 2A (32)). Additional sites important for kinase modulation of PR signaling such as Ser345 were also rapidly phosphorylated in response to R5020 and progesterone (Fig. 2C; Supplemental Fig. 2B (32)), suggesting that PR isoforms expressed in hFTE cells were properly folded and functional with regard to rapid induction of signaling pathways and subsequent phosphorylation events.

To verify downstream ligand-induced transcriptional repression/activation in these lines, the regulation of select PR target genes previously identified by our laboratory in ES-2 OC cell models was examined (8). Quantitative RT-PCR analyses showed concentration-dependent progestin- or progesterone-induced downregulation (ie, transcriptional repression) of interleukin-1β mRNA in PR-A+ and PR-B+ hFTE cells at 6 hours and upregulation (ie, transcriptional activation) of NEDD9 mRNA at 48 hours, with no change observed in EV cells at either time point (Supplemental Fig. 2C (32)). Analyses of multiple PR+ clones showed similar regulation of these genes and revealed PR-A-dominant downregulation of interleukin-8 mRNA at 6 hours (Supplemental Fig. 2D (32)) and PR-B-specific upregulation of FOXO1 mRNA at 48 hours of progestin or progesterone treatment (Supplemental Fig. 2E (32)).

PR and Progestins Promote Cell Behaviors That Support Cancer Phenotypes

Mutations acquired within fallopian tube epithelia can lead to cell survival, proliferation, cell-cell aggregation/disaggregation, and other cell behaviors that can support disease progression (11, 12, 48). The effect of PR expression and progestin treatment on phenotypes that could promote such processes was examined. The initial characterization of proliferation was analyzed using an ATP-based assay that allowed for high-throughput measurement of rate of change over time in numerous clones. The expression of PR-A alone led to enhanced proliferation as compared to EV and PR-B+ hFTE (Fig. 2D). In addition, these cells also exhibited greater migratory capacity in transwell migration assays in the presence of 10% FBS (ie, as the chemoattractant; Fig. 2E). Signaling in the absence of hormone (ie, ligand-independent*; unliganded*) is a common feature of steroid receptors, including PR, and is as important as their ligand-dependent (*liganded*) actions (21, 22).

The ability of progestins to mediate FTE cell fate through the regulation of cell cycle progression was studied in these hFTE lines. Cellular analyses of indices of proliferation (Ki67), senescence (β-galactosidase; β-gal), and DNA synthesis (BrdU incorporation) were employed in parallel samples using immunofluorescence assays. Treatment with R5020 for 72 hours resulted in a decrease in proliferative cells in the PR+ hFTE, visualized by a decline in Ki67+ cells along with an increase in senescence-associated β-galactosidase (SAβ-gal)+ cells (Fig. 2F; immunofluorescence images-Supplemental Fig. 3A (32)). A coincident decrease in DNA synthesis also occurred, observed as a decline in BrdU+ cells (Fig. 2F; immunofluorescence images-Supplemental Fig. 3B (32)). Additionally, flow cytometry analyses showed that, within 24 hours, these cells were pushed into G0/G1 with concomitant decrease in the percentage of cells in S phase (Fig. 2G). This inhibition, however, did not appear to be a state of terminal arrest (senescence) since serum stimulation for 24 to 48 hours following progestin treatment resulted in a recovery of proliferative Ki67+ cells (Fig. 2H). Exposure to serum for several days following this cell cycle arrest led to a steady increase

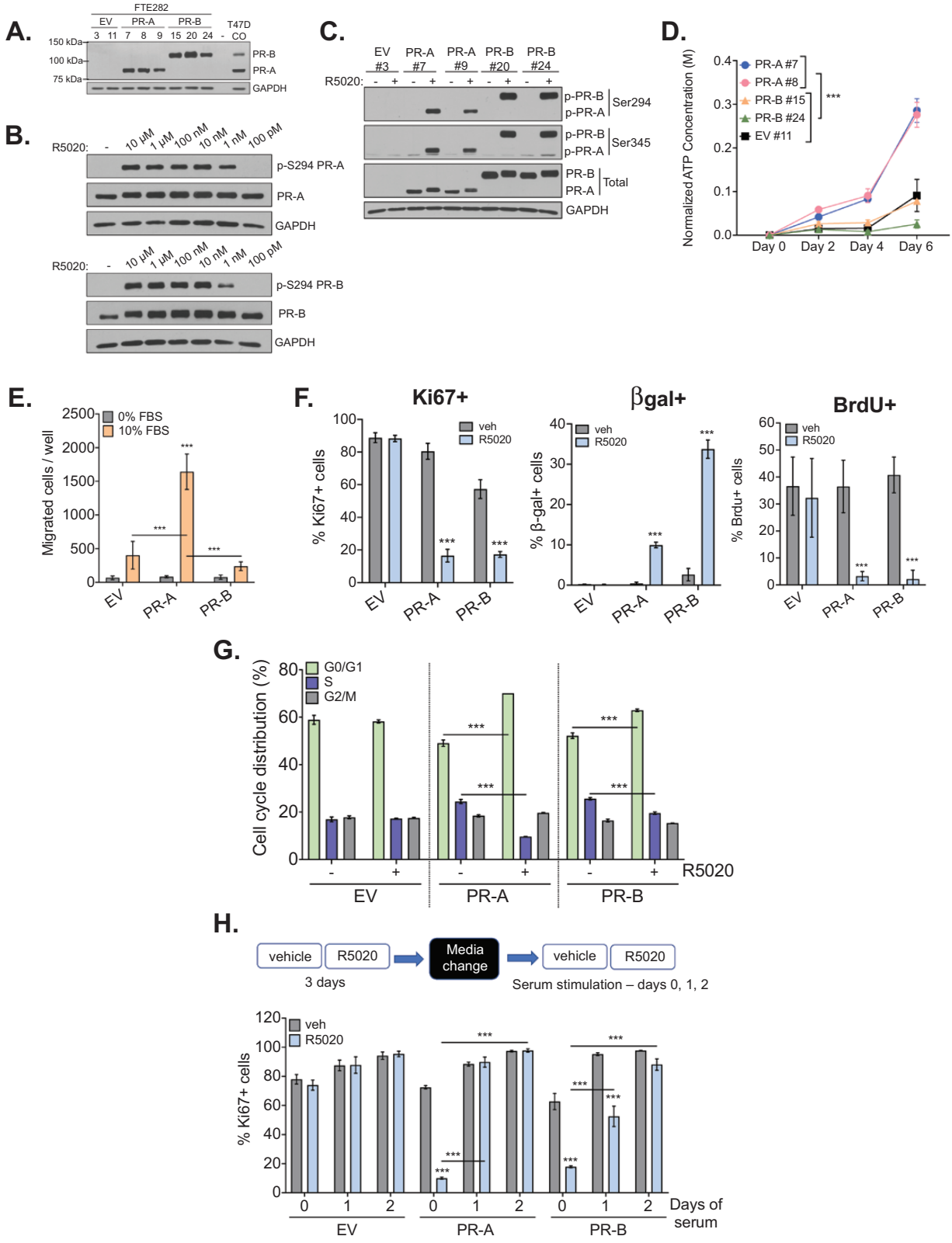

Figure 2. Novel PR-expressing human fallopian tube epithelia (hFTE) show functional PR signaling and progestin-mediated cell cycle arrest. **A,** PR expression in empty vector (EV), PR-A+, and PR-B+ hFTE clonal lines; T47D CO cells as a positive control. **B,** Phosphorylation of PR at Ser294 in hFTE PR-A+ (#7) and PR-B+ (#24) clones following vehicle (–) or varying concentrations of R5020 (1 hour). **C,** Phosphorylation of PR at Ser294 and Ser345, in hFTE following vehicle (–) or R5020 (+; 10nM; 1 hour). **D,** Proliferation of hFTE EV #11, PR-A #7, #8, and PR-B #15, #24 over 0, 2, 4, and 6 days. **E,** Transwell migration of hFTE EV #11, PR-A #7, and PR-B #24 in response to 0% (control) or 10% FBS for 18 hours. **F,** Percentage of hFTE cells positive for Ki67, SAβ-gal, and BrdU (cells/field) following treatment with vehicle (veh) or R5020 (10nM; 72 hours). **G,** Cell cycle analyses (FACS) of hFTE treated with vehicle (veh) or R5020 (10nM; 24 hours). **H,** Percentage of positive Ki67 hFTE cells after 0 to 2 days serum stimulation. Treatment of cells for 3 days with vehicle or R5020, followed by a change to media containing FBS (no R5020) for 0-2 days (schematic). Graphs represent the mean ± SD, ***$P < 0.001$ (n = 3).

in cell numbers (Supplemental Fig. 3C (32)). These studies demonstrate that progestins are able to promote G0 cell cycle arrest in PR+ hFTE that is fully reversible.

The ability of progestins to support the formation of tumor emboli (ie, spheroids), a process important for dissemination, was also examined. R5020 treatment robustly promoted cell-cell aggregation with larger, compact spheroids observed for PR-A+ and PR-B+ hFTE (Fig. 3A). In contrast, no PR expression (EV hFTE) or the absence of progestins (vehicle) resulted in looser, smaller structures (Fig. 3A). To simulate the disaggregation/reaggregation thought to occur during dissemination of early FTE lesions (49, 50), these structures were dissociated and reseeded without treatments. Spheroid formation under these conditions only occurred in the PR+ hFTE cells treated with R5020 during the initial aggregation (Fig. 3B). No discernable structures were evident for EV hFTE or for PR-A+ or PR-B+ hFTE cultured with vehicle only. Importantly, aggregation experiments were also conducted with an additional cell model. Immortalized murine oviductal epithelial (MOE) cells, expressing low endogenous levels of both PR-A and PR-B (inset, Fig. 3C), also exhibited enhanced spheroid formation with R5020 treatment (Fig. 3C).

Notably, treatment of cells with the PR antagonists, onapristone (Ona) or RU486, did not block PR-driven spheroid formation and, similar to R5020 (ie, a PR agonist), both compounds supported cell aggregation (Supplemental Fig. 4A (32)). Analysis of S294 phosphorylation revealed that onapristone and RU486 were unable to block R5020-induced PR phosphorylation and acted instead as partial agonists, inducing phosphorylation at the S294 residue (Supplemental Fig. 4B (32)). These antagonists are effective in blocking R5020 effects in breast cancer lines (19), suggesting unique actions of these compounds that may be specific to the hFTE cell type and/or the state of these cells. Interestingly, it is well known that PR antagonists like RU486 acquire partial agonist activity in a background of elevated cyclic adenosine monophosphate (cAMP) activity (51) and that selective estrogen receptor modulators such as tamoxifen also tend to have agonistic actions in reproductive tissue like the uterus, contrary to its antagonistic actions in the breast (52). The basis for this reversal of antagonist to agonist action is unknown, but likely involves activation of rapid signaling pathways (cAMP, MAPKs) known to modify nuclear steroid receptors, such as hormone-binding membrane estrogen receptors (mERs, GPER) and membrane PRs (mPRs or PAQRs, PGRMC1) also highly expressed in the reproductive tract (53, 54).

Epithelial cells within FT lesions can be shed, aggregate into emboli, and potentially go on to invade the layer lining the peritoneal cavity (55, 56). Interaction with the abundant collagen type I layer beneath the mesothelium is important for OC cell attachment, motility, and invasion (50, 57). To determine the effect of PR signaling on a similar cell behavior, we utilized a simplified model of collagen invasion where our hFTE lines were cultured in the absence or presence of R5020 to form spheroids, encased in a collagen type I matrix, then allowed to invade for 72 hours. Remarkably, we observed heightened invasive behavior that was fully dependent on PR expression and the presence of R5020 during spheroid formation (Fig. 3D). Similar to what was observed with spheroid formation, the activation of PR by progestin was necessary to support this invasive behavior.

Gene Expression Profiling of PR+ hFTE Highlights Unique Regulation

To define the potential pathways transcriptionally regulated by PR and progestins that could drive these cancer-like phenotypes, RNAseq analyses was performed on EV and PR+ hFTE treated with vehicle or R5020 for 6 and 48 hours. Representative Venn diagrams (Fig. 4A) and heat maps were created to analyze the resulting transcriptomes via either unsupervised (Supplemental Fig. 5A (32)) or supervised clustering (ie, by treatment; Supplemental Fig 5B (32)). In the absence of progestin, cells expressing either PR-A or PR-B regulate distinct gene clusters relative to the same parental cells expressing EV. Surprisingly, however, simply the expression of PR-A in the absence of R5020 dramatically altered the transcriptome, activating over 400 genes and repressing over 500 genes at both time points relative to both untreated EV or PR-B+ cells (Fig. 4A; PR-A = blue, PR-B = yellow). The addition of ligand to PR-A+ cells induced only subtle further changes in gene expression; compare all PR-A gene sets to all EV or PR-B gene sets (Supplemental Fig. 5A (32)) and compare gene sets in lanes 1 and 2–3 or lanes 6 and 7–8 (Supplemental Fig. 5B (32)). Ligand-independent actions of PR-A as measured by changes in global gene expression have also been reported in breast (18) and ovarian cancer (9) models but unliganded PR-A was predominantly repressive in these cancer contexts. In sharp contrast to PR-A expression, the expression of PR-B in the absence of ligand was most similar to EV (Supplemental Fig. 5A (32); far right cluster). Strikingly, the addition of R5020 to PR-B+ cells, especially at 48 hours, dramatically altered gene expression (Fig. 4A; 808 upregulated genes, 572 downregulated genes) relative to vehicle controls. This is also evident in Supplemental Fig. 5B (32); compare supervised clustering of lanes 4 and 5 or lanes 9 and 10. These data suggest that similar to both breast and ovarian cancer models (9, 58), PR-B is the dominant hormone-regulated (ie, hormone-sensitive) isoform,

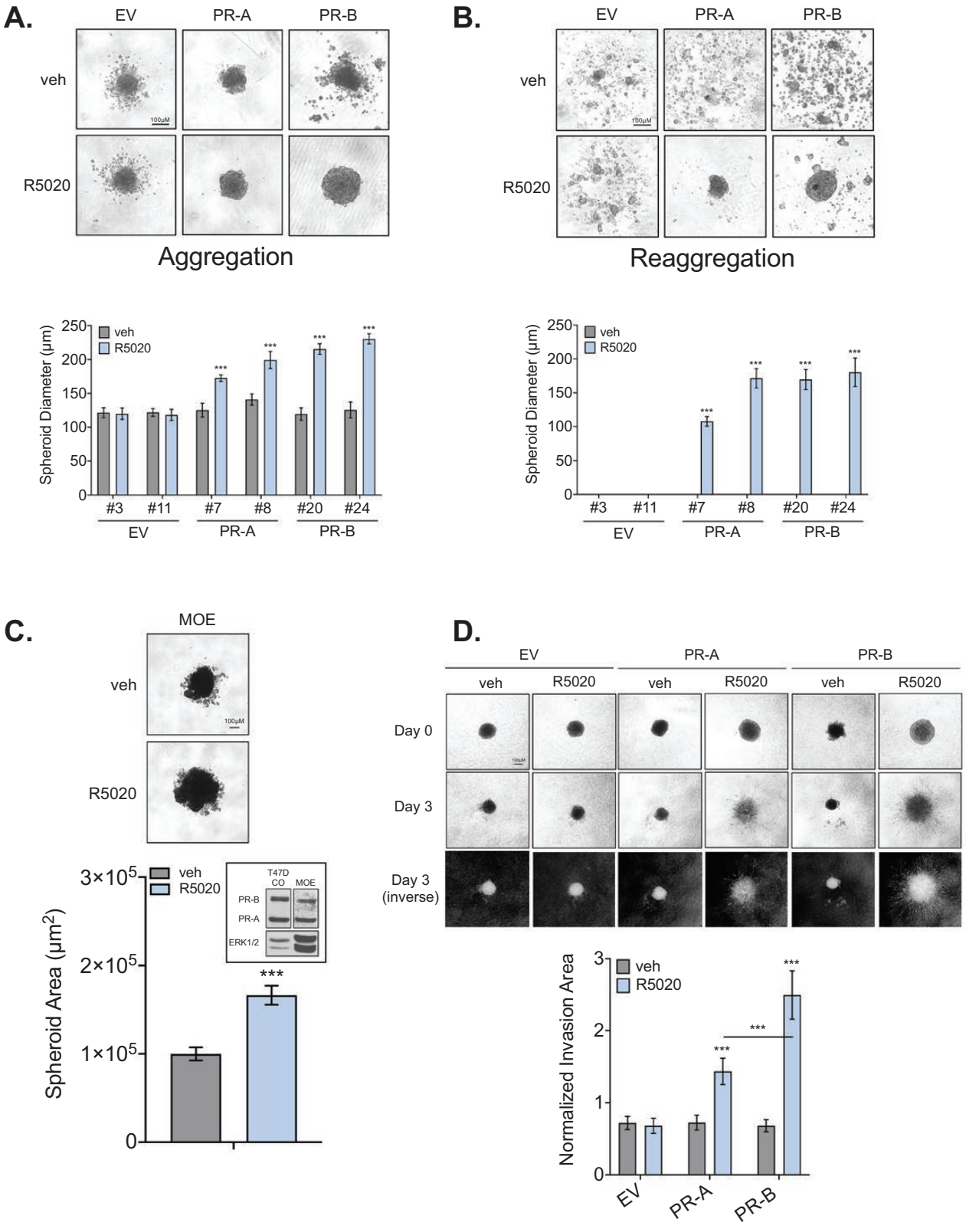

Figure 3. PR and progestins promote cell behaviors that support cancer phenotypes. **A-B,** Representative bright-field images and average diameter of primary aggregated **(A)** and secondary dispersed and reaggregated (**B)** spheroid cultures of hFTE treated with vehicle (veh) or R5020 (10nM; 72 hours). No treatments were included in secondary cultures. **C,** Bright-field images and average area of murine oviductal epithelium (MOE) spheroid cultures treated with vehicle (veh) or R5020 (10nM; 72 hours) graphed. *Inset,* PR expression in MOE cells with T47D CO cells as positive control. ERK1/2 shown as loading control. **D,** Collagen invasion assay of hFTE spheroid cultures generated under vehicle (veh) or R5020 (10nM; 72 hours) treatment, then embedded into collagen for 72 hours without treatments. Bright-field images after 0 and 3 days of invasion. Inverse Day 3 images below. Normalized invasion area was calculated as described in methods and represented in graph. Graphs represent mean ± SD, ***$P < 0.001$ (n = 3).

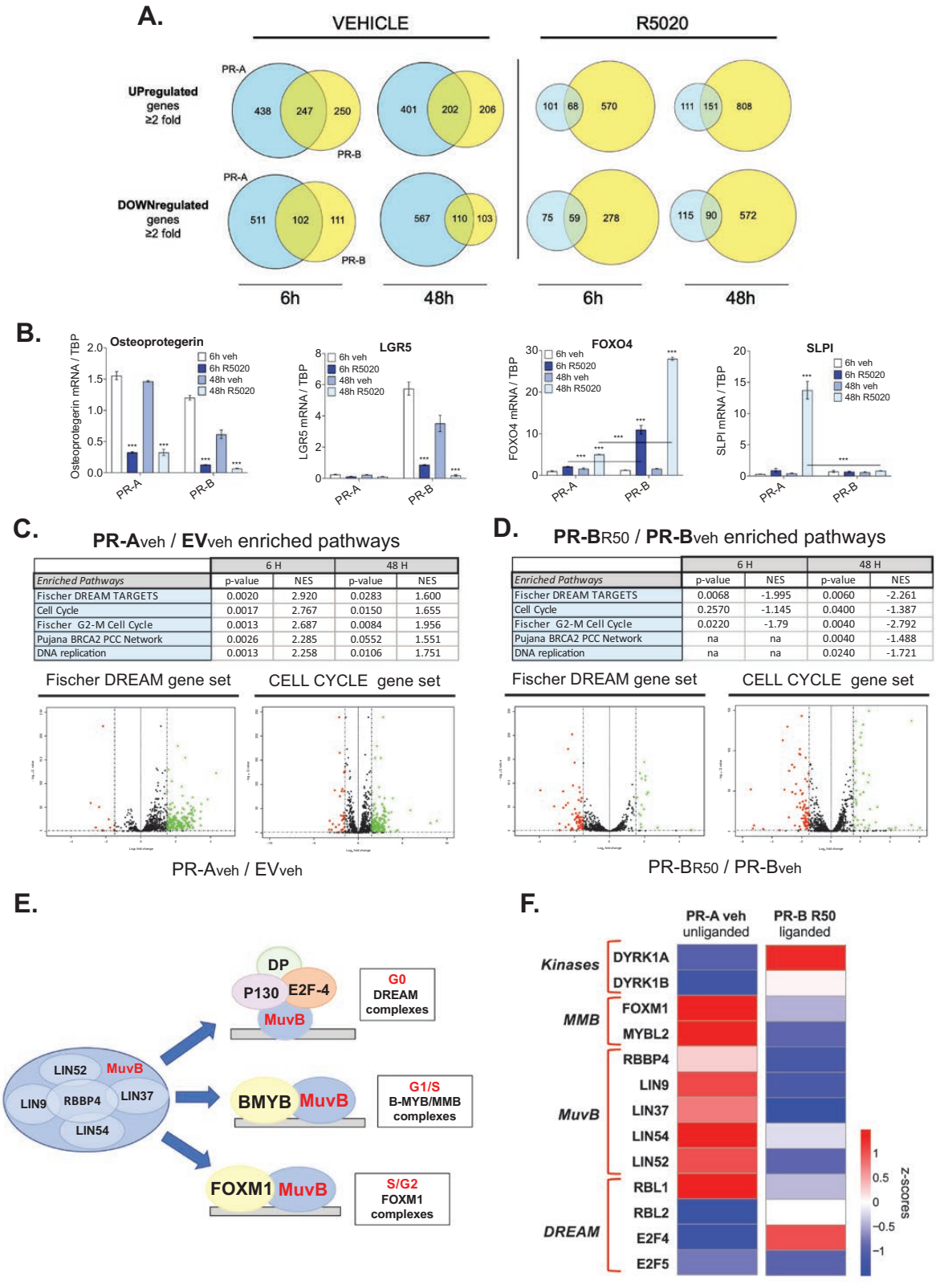

	6 H		48 H	
Enriched Pathways	p-value	NES	p-value	NES
Fischer DREAM TARGETS	0.0020	2.920	0.0283	1.600
Cell Cycle	0.0017	2.767	0.0150	1.655
Fischer G2-M Cell Cycle	0.0013	2.687	0.0084	1.956
Pujana BRCA2 PCC Network	0.0026	2.285	0.0552	1.551
DNA replication	0.0013	2.258	0.0106	1.751

	6 H		48 H	
Enriched Pathways	p-value	NES	p-value	NES
Fischer DREAM TARGETS	0.0068	-1.995	0.0060	-2.261
Cell Cycle	0.2570	-1.145	0.0400	-1.387
Fischer G2-M Cell Cycle	0.0220	-1.79	0.0040	-2.792
Pujana BRCA2 PCC Network	na	na	0.0040	-1.488
DNA replication	na	na	0.0240	-1.721

Figure 4. Gene expression profiling of hFTE highlights unique regulation. **A,** Venn diagrams representing common, isoform-specific and intersecting gene sets in the absence of progestins (LEFT: vehicle; unliganded) or presence of progestins (RIGHT: R5020; liganded) at 6 and 48 hours. BLUE circles depict PR-A gene sets and YELLOW circles depict PR-B. Upregulated sets are on TOP; downregulated on BOTTOM. Cutoff for DEGs was ≥2 fold. **B,** Osteoprotegerin (TNFRSF11B), LGR5, FOXO4 and secretory leucocyte peptidase inhibitor (SLPI) mRNA expression in hFTE pools, vehicle (veh) or R5020 (10nM) for 6 or 48 hours treatments. Graphs represent mean ± SD, ***$P < 0.001$ (n = 3). **C,** Enriched pathways analyses of 6-hour and 48-hour vehicle-treated (unliganded) PR-A+ hFTE (PR-Aveh vs EVveh; table) and DREAM and Cell Cycle volcano plots for PR-A+ hFTE (unliganded; veh, 6

while PR-A mediates significant ligand-independent actions. The major contrast between hFTE and breast or ovarian cancer models lies in the direction and magnitude of gene regulation, with unliganded PR-A strongly activating a significant number (>400 at both time points) of genes and liganded PR-B strongly repressing a large subset (~572 at 48 hours) of genes in PR+ hFTE models (Fig. 4A and Supplemental Fig. 5 (32)); PR-B primarily activates genes in the presence of ligand while PR-A is dominantly repressive regardless of ligand in breast and ovarian cancer models (9).

The progestin and PR-dependent regulation of known PR target genes was independently validated by RT-qPCR (Fig. 4B). Importantly, both common and isoform-specific genes are progestin-regulated, as illustrated in Fig. 4B and Supplemental Fig. 6A (32). Downregulation of the soluble decoy receptor of RANK, osteoprotegerin (TNFRSF11B gene; OPG), was observed for both isoforms, in contrast to PR-B-specific downregulation of the canonical Wnt receptor, LGR5, and greater upregulation of the forkhead transcription factor, FOXO4, as compared to PR-A. PR-A isoform-specific gene regulation was also observed, including such genes as the secretory leucocyte peptidase inhibitor, *SLPI*, which is known to be highly expressed in normal cervix and fallopian tube (59). These observations suggest that exogenously expressed PRs in hFTE cells appropriately model endogenous PR actions at known PR target genes (60-62).

Regulation of both common and isoform-specific PR target genes in hFTE cells suggests important shared functions as well as significant functional differences between PR isoforms. Pathway enrichment analysis was performed to determine what specific biological processes were significantly regulated by either PR-A or PR-B. Interestingly, cell cycle progression pathways were greatly enriched in PR+ hFTE cells (Fig. 4C, D; Supplemental Fig. 6B (32)). A top pathway observed in unliganded PR-A+ hFTE, as well as liganded PR-B+ hFTE, was the DREAM pathway, encompassing the target genes regulated by the DREAM complex which modulates G0 cell cycle arrest. Notably, PR-A and PR-B isoforms exhibited opposing effects: in the absence of progestin, DREAM target genes, including cell cycle pathways, were activated in PR-A+ hFTE cells, consistent with permissive cell cycle progression (see Fig. 2D). However, these pathways were potently deactivated in progestin-treated PR-B+ hFTE (and to a lesser extent in progestin-treated PR-A+ hFTE), indicative of cell cycle blockade, perhaps via DREAM activation. Activated DREAM complexes collectively target and repress ~900+ genes which include critical G1/S and G2/M cell cycle genes, p53 target genes, as well as many other cell cycle dependent genes (63). Volcano plots of Fischer DREAM and Cell Cycle gene sets illustrate the enrichment of such target genes, along with their isoform-specific (ie, opposing directions) and shared hormone-dependent regulation (Fig. 4C and 4D). In addition, a heatmap of differentially expressed genes critical for DREAM function reveals that PR expression (PR-A) and progestin treatment (PR-B) can regulate genes encoding the protein components of the DREAM complex itself (RBBP4, E2F4/5, LIN9/37/52/54, RBL1/2), genes encoding the kinases that modulate the formation of this complex (DYRK1A/B), along with genes for the components of those complexes that promote the re-entry into the cell cycle (FOXM1, MYBL2; Fig. 4F; schematic of cell cycle complexes Fig. 4E). Of note, is the strong upregulation of DREAM target genes such as FOXM1 and MYBL2 and other proteins of the MuvB complex in unliganded PR-A+ cells—such regulation would be expected to enhance the progression through G1/S/G2 phases of the cell cycle (*left heatmap*; PR-A vehicle vs EV control). In contrast, many of these same genes are potently repressed in liganded PR-B hFTE with R5020 treatment, presumably promoting cell cycle arrest (*right heatmap*; PR-B R50 vs PR-B vehicle).

In addition to cell cycle progression pathways, other pathways that may be relevant to our observed cellular phenotypes were enriched in our PR+ hFTE models including cell-cell/cell-matrix adhesion, cell morphogenesis, Wnt signaling, oxidation-reduction activity, and stem cell differentiation (Supplemental Fig. 6B (32)). For example, PR-A–enriched pathways included DNA replication in the absence of progestin and stem cell differentiation in the presence of progestin. This is consistent with our finding that PR-A+ hFTE cells have an increased rate of growth relative to EV cells (Fig. 2). PR-B–enriched pathways included numerous pathways associated with cell shape, regulation of

Figure 4: continued

hours). **D,** Enriched pathways analyses at 6 and 48 hours of R5020-treated (liganded) PR-B+ hFTE (PR-Br50 vs PR-Bveh; table) and DREAM and Cell Cycle volcano plots for PR-B+ hFTE (liganded; R5020 48 hours). **E,** Schematic of protein complexes during cell cycle arrest and progression showing the foundational MuvB complex on the left which during the transition from G0 to G1/S through S/G2 associates/disassociates with partners such as DREAM-specific proteins and others pictured. **F,** Changes in gene expression in response to unliganded PR-A or liganded PR-B. Differential expression of genes encoding specific DREAM complex proteins, B-MYB/MMB or the MuvB complexes or kinases that regulate DREAM assembly are included. Left column represents changes (z-scores) in PR-A+ hFTE treated with vehicle at 6 hours (EV vs PR-A). Right column represents changes in PR-B+ hFTE treated with R5020 at 48 hours (PR-Bveh vs PR-B R5020). Gene names, bracketed by their complex or function, are indicated to the left of heatmaps.

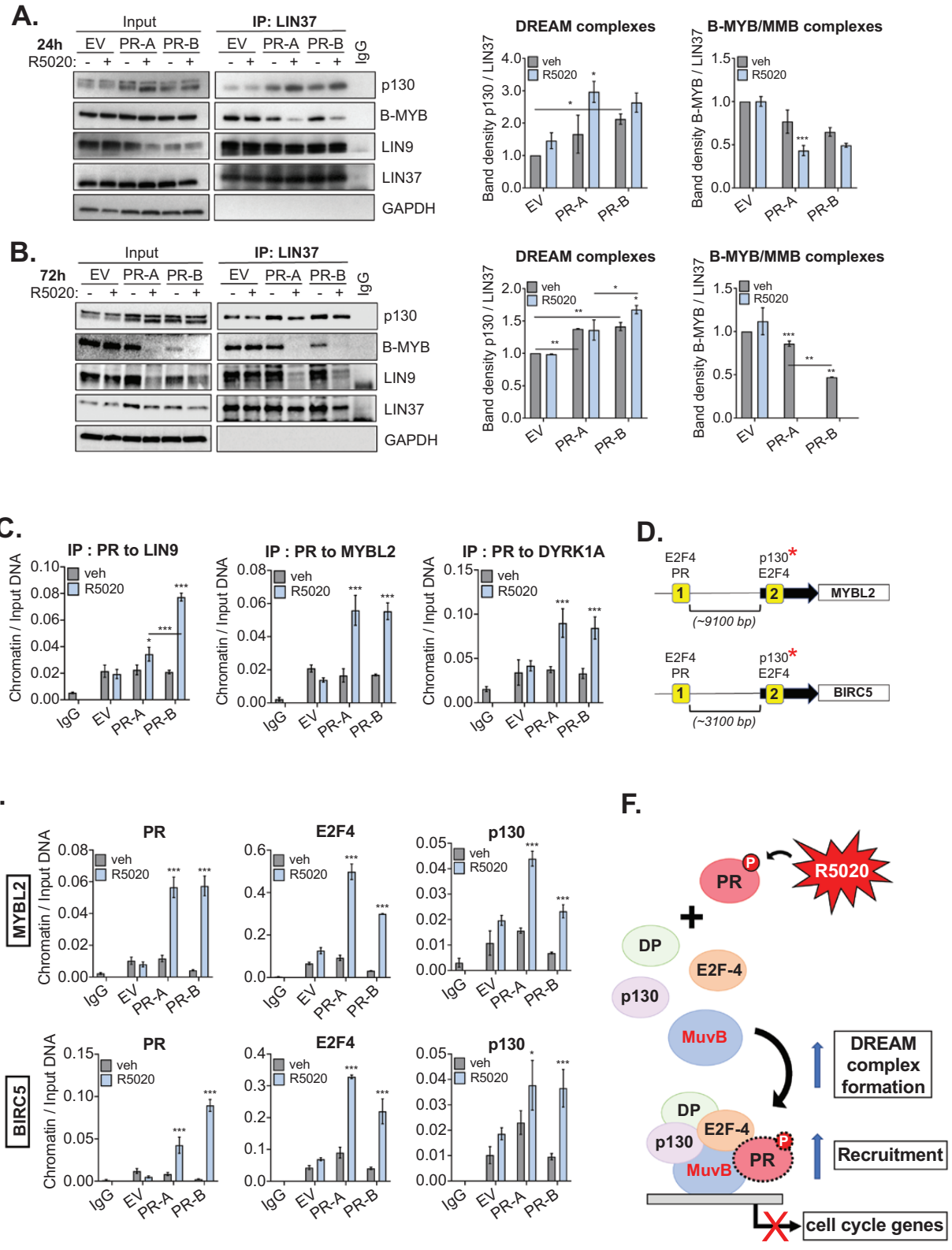

Figure 5. Progestins promote quiescence in hFTE cells through modulation of the DREAM complex. **A,** Immunoprecipitated proteins (IP) of LIN37 in hFTE following 24 hours and **B,** 72 hours of treatment with vehicle (-) or R5020 (+; 10nM). Left blot = input cell lysates; right blot = IP from these lysates plus IgG control. Lanes L to R: hFTE EV vehicle (-) or R5020 (+); hFTE PR-A (-)/(+); hFTE PR-B (-)/(+). GAPDH shown as loading control. Expression of LIN 9 and LIN37 as core MuvB complex proteins, p130 as DREAM-specific protein, and BMYB as G1/S complex protein was determined. DREAM complexes (G0 state) were quantified using the band density ratio of p130/LIN37. B-MYB/MMB complexes (G1/S progression) were quantified using

cell projections and adhesions in the absence of ligand and amino acid metabolism and cytokine signaling in the presence of progestin. Again, these findings are consistent with our finding that PR-B+ hFTE cells are more invasive relative to PR-A+ cells (Fig. 3D). Interestingly, consistent with strong enrichment of cell cycle pathways, both isoforms also regulate p53- and BRCA2-associated pathways in the absence (PR-A) or presence (PR-B) of progestin.

Progestins Modulate DREAM Complex Formation and Recruitment

RNAseq analyses indicated that the target genes of the DREAM complex were robustly enriched in PR+ hFTE models. During arrest in G0, the expression of these cell cycle-dependent genes is actively repressed by the DREAM complex, which consists of the DREAM-specific proteins, **D**imerization partner DP1/2, **R**b-like p130/p107, **E**2F4/5 **A**nd the **M**uvB core complex (LIN9, LIN37, LIN52, LIN54, RBBP4 proteins (27)). During the transition from G0 into late G1/early S, this transcriptional repression is lifted by dissociation of DP1/2, p130 and E2F4/5 from the MuvB core. This is followed by association of the MuvB core with B-MYB, together known as the B-MYB/MMB complex, in G1/S phase. In order to determine if progestins induce cell cycle arrest/quiescence (see Fig. 2) via regulation of the formation of the DREAM and B-MYB/MMB complexes, EV and PR+ hFTE cells were treated with R5020 and complexes were immunoprecipitated using a LIN37 antibody. The relative formation of DREAM (p130/LIN37 ratio) and B-MYB/MMB complexes (B-MYB/LIN37 ratio) was quantified by blotting for p130, B-MYB, LIN9, and LIN37. Progestins (24-hour) enhanced the formation of DREAM complexes and decreased B-MYB/MMB complexes in PR-A+ hFTE, while progestin-treated PR-B+ cells followed a similar trend (Fig. 5A). At 72 hours, progestin treatment resulted in further enhanced DREAM complex formation, with a total loss of B-MYB/MMB complexes (Fig. 5B). In addition, at this time point, the amount of B-MYB protein was dramatically reduced in the input pellets, along with LIN9, supporting the RNAseq results, which revealed that activation of PR signaling modulates expression of DREAM and B-MYB/MMB complex subunits (see Fig. 4E and 4F). In contrast, at 24 hours, the amount of input B-MYB protein was unchanged in vehicle and R5020 treated cells yet B-MYB/MMB complex formation was reduced with progestins, supporting the actions of activated PR isoforms to influence complex formation. When these complexes were analyzed in PR+ hFTE that were treated with serum for 24 hours to initiate the reversal of the progestin-induced G0 arrest (see schematic in Fig. 2H), the slower growing isoform PR-B+ hFTE shows a further increase in DREAM complexes (Supplemental Fig. 7A (32)). A basal level of DREAM complexes was observed in the unliganded PR-A+ and PR-B+ hFTE lysates. This could reflect the ability of PR, in the absence of progestins, to modulate DREAM complex interactions with its own subunits and/or other proteins, potentially inhibiting DREAM-mediated repression.

RT-qPCR analyses of R5020-treated PR-A+ and PR-B+ hFTE cells confirmed that MYBL2 mRNA, the gene encoding the B-MYB protein, and LIN9 mRNA were downregulated as well as FOXM1 mRNA, which encodes the transcription factor that associates with MuvB during the transition to G2/M phase (Supplemental Fig. 7B (32)). In addition, DYRK1A mRNA, which encodes a kinase that regulates DREAM complex assembly, was upregulated in PR-B+ hFTE. ChIP analyses confirmed that, following progestin treatment for 3 hours, PRs are recruited to progesterone receptor binding sites (PRE) in the promoters of LIN9, MYBL2, and DYRK1A (Fig. 5C). No change in relative mRNA levels or PR recruitment was observed for these genes in the EV hFTE cells (Fig. 5C).

Interestingly, additional ChIP analyses revealed that PR is co-recruited along with DREAM complex proteins to target genes. A PRE site in both the DREAM target genes, MYBL2 and BIRC5, overlaps with an E2F binding site and, as expected, PR and E2F4 are recruited to the same region following a 3-hour R5020 treatment, with no change observed in p130 (Fig. 5D schematic—site #1; data—Supplemental Fig. 7C (32)). A secondary site within the promoter of these genes contains consensus E2F binding elements and is known to recruit only E2F4, with p130 as a cofactor, but not PR (Fig. 5D; schematic—site #2 with

Figure 5: continued

the band density ratio of BMYB/LIN37. See Fig. 4E for schematic of complexes. **C,** Chromatin immunoprecipitation (ChIP) assays of PR recruitment to progesterone response elements (PRE) present in LIN9, MYBL2 and DYRK1A genes after vehicle (veh) or R5020 (10nM; 3-hour) treatment. **(D-E)** ChIP assays of PR, p130, and E2F4 recruitment to shared and unique sites within DREAM target genes. **D,** Schematic of the MYBL2 and BIRC5 genes with site #1 containing overlapping response elements (RE) for PR and E2F4 and site #2 containing RE for E2F4 only with p130 acting as a known cofactor. Approximate distance between sites and the promoter of each gene is indicated. **E,** ChIP assay of site #2 following treatment with vehicle (veh) or R5020 (both D & E: 10nM; 3 hours). **F,** Progestins promote quiescence in PR+ hFTE by increasing DREAM complex formation and increasing recruitment to DREAM complex target genes, resulting in a repression of cell cycle gene transcription. Graphs represent mean ± SD, $*P < 0.05$, $**P < 0.01$, $***P < 0.001$ (n = 3).

asterisk). Yet, our data demonstrated that all 3 proteins show enhanced recruitment to this site with R5020 treatment (Fig. 5E). No significant change in recruitment was observed in the EV hFTE cells. In addition, analyses of 72-hour DREAM immunoprecipitations indicates that PR protein is present and progestin treatment enhanced PR association, in particular, for the PR-B isoform (Supplemental Fig. 7D (32)).

Taken together, these results suggest that progestins promote G0 arrest through modulation of and interaction with the DREAM complex assembly (Fig. 5F). Activation of PR by the progestin, R5020, leads to increased DREAM complex formation and increased recruitment of the repressive DREAM complex, including PR, to the regulatory elements of the DREAM target genes. PR recruitment to these genes also results in the regulation of the expression of critical DREAM and B-MYB/MMB complex proteins which, in concert with enhanced DREAM complex formation, leads to potent repression of cell cycle gene sets and the observed block in cell cycle progression.

Manipulation of DREAM Function and DYRKs Attenuates the Effects of PR Signaling in hFTE Cells

To validate the above findings in an independent FTE model and further explore the connection between the progestins' effects on FTE and DREAM complex modulation, we created an additional model of PR-expressing FTE using the human fallopian tube epithelial cell line UWFT.1681, originally immortalized with the HPV E6/E7 proteins (Fig. 6A). The HPV E7 oncoprotein is known to interfere with DREAM function by promoting the degradation of the p130 protein (64, 65). Western analysis of DREAM and B-MYB/MMB complex proteins in either whole cell lysates (input) or Lin37 immunoprecipitates verified that these lines express very low p130 protein as compared to the hFTE model (Supplemental Fig. 8A (32); red arrowheads, left hFTE vs right UWFT). Given the loss of p130 in this model, we anticipated that progestins' actions should be attenuated or abolished in these cells, if dependent on DREAM function. Treatment of EV, PR-A+, and PR-B+ UWFT.1681 cells with R5020 (10 nM, 24 hours) failed to halt cell cycle progression in these E6+/E7+ models. In sharp contrast to our hFTE cells, no G0/G1 arrest was observed and no decrease in percentage of cells in S phase occurred (Fig. 6B). Additional experiments with 48 and 72 hours of R5020 treatment yielded similar results (data not shown). Accordingly, transcriptional repression of MYBL2, LIN9, and FOXM1 mRNA expression was abolished in PR-A+ and strongly attenuated in PR-B+ UWFT.1681 cells (Fig. 6C), as compared to PR+ hFTE (see Supplemental Fig. 7B for hFTE data (32)). This is supported by the Western analysis that showed little to no downregulation of B-MYB (MYBL2 gene) or LIN9 protein expression observed following R5020 treatment (Supplemental Figure 8A (32); blue arrowheads, left hFTE vs right UWFT). However, aggregation/reaggregation cultures revealed that R5020 treatment could still promote primary spheroid formation in this model (Supplemental Fig. 8B (32)) and was required for reaggregation and spheroid formation following dispersal and reseeding of the primary cultures (Fig. 6D). In addition, progestins enhanced collagen invasion for both PR-A+ and PR-B+ UWFT.1681 cells (Fig. 6E). These data indicate that PR exerts similar effects on cell aggregation/spheroid formation and collagen invasion in multiple independently derived hFTE cell models. Remarkably, loss of p130 (ie, via HPV infection/expression of E6/E7) abrogates PR-driven cell cycle arrest but allows the expression of other progesterone/PR-driven ovarian cancer cell phenotypes.

Alterations in the expression of genes encoding members of the Myb-MuvB complex are associated with prognostic markers of aggressiveness in some cancers (27). In addition, such dysregulation of the DREAM complex may be tied to disease recurrence due to its role in maintaining quiescence. As such, the value of targeting transcriptional complexes that regulate cell cycle exit, such as the DREAM complex, is being actively explored (66, 67). Dual-specificity tyrosine phosphorylation-regulated kinases (DYRKs) are enzymes which are activated by autophosphorylation and go on to phosphorylate serine and threonine residues of target proteins (68). Like p130, the class I DYRKs, DYRK1A, and DYRK1B, are negative regulators of the cell cycle. DYRK1A, in particular, is known to phosphorylate LIN52 (a MuvB subunit protein) allowing for the association of p130 and MuvB and subsequent DREAM complex assembly (69). The actions of DYRK1B also support the quiescent state by phosphorylating LIN52 (69, 70). As a pharmacologic means to block DREAM and determine if DYRK1 kinases are required mediators of progestin-induced quiescence, we tested the potential chemotherapeutic drug, harmine, in the PR+ hFTE lines. Harmine is a naturally occurring β-carboline alkaloid and inhibitor of class I DYRK kinase activity (71) that interferes with DREAM assembly and entrance into G0 (72). As expected, harmine treatment inhibited the accumulation in G0/G1 observed in both PR-A+ and PR-B+ hFTE following progestin treatment (Fig. 7A). This treatment also resulted in a greater percentage of cells in G2/M. The dependence of PR transcriptional signaling on DYRK1 activity is also supported by harmine's ability to lift the R5020-dependent transcriptional repression of

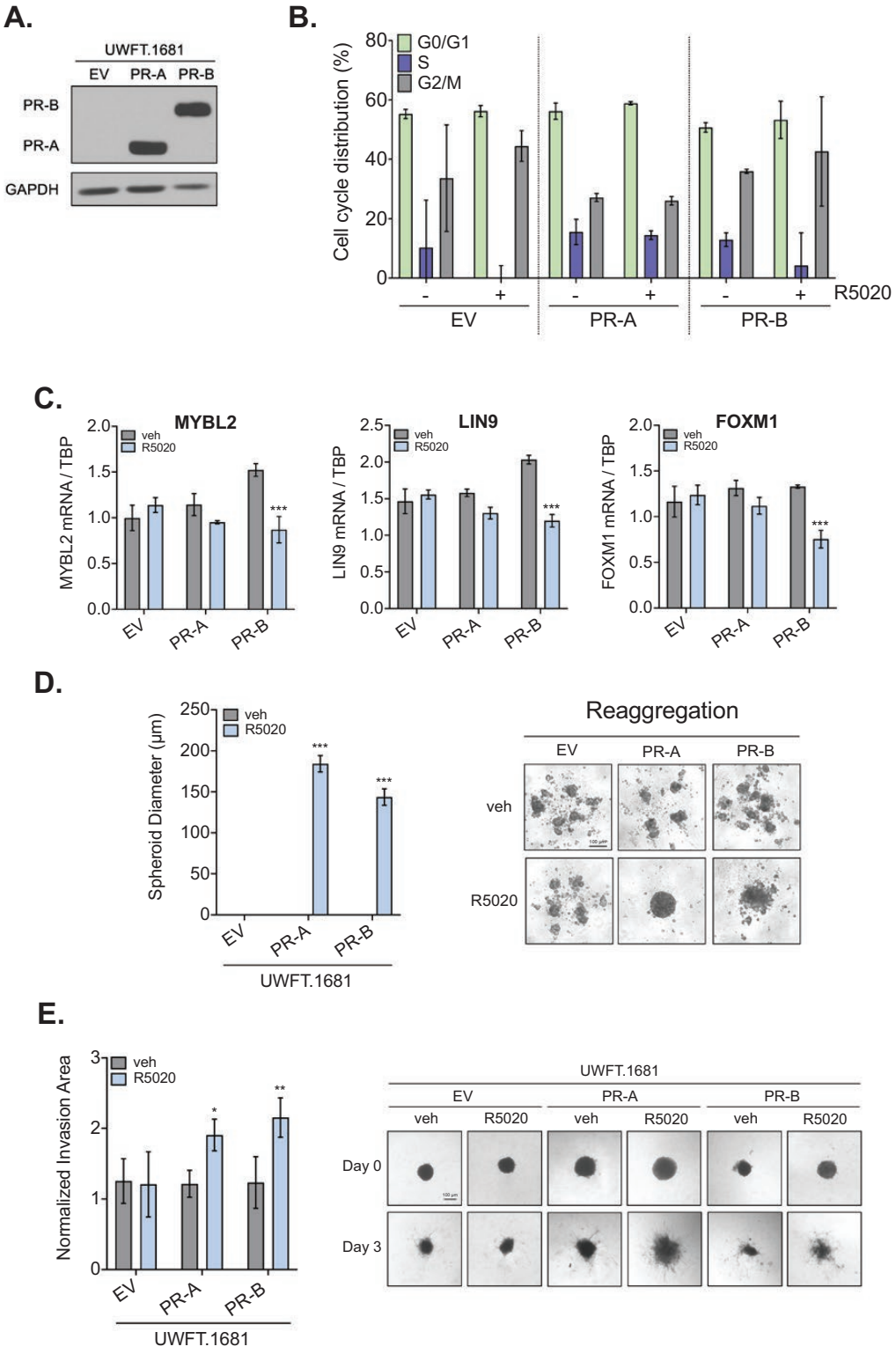

Figure 6. Progestin-induced effects are altered in a cell model deficient in DREAM complex formation. **A,** PR expression in empty vector (EV), PR-A+, and PR-B+ UWFT.1681 pools. GAPDH shown as loading control. **B,** Cell cycle analyses (FACS) of UWFT.1681 cells treated with vehicle (veh) or R5020 (10nM; 24 hours). **C,** Transcriptional regulation of MYBL2, LIN9, and FOXM1 mRNA in PR+ UWFT.1681 with vehicle (veh) or R5020 (10nM) for 72 hours. **D,** Average diameter of secondary reaggregated spheroid cultures of UWFT.1681 cells treated as in C. **E,** Collagen invasion assay of UWFT.1681 spheroid cultures generated under vehicle (veh) or R5020 (10nM; 72 hours) treatment, then embedded into collagen for 72 hours without treatments. Representative bright-field images after 0 and 3 days of invasion and normalized invasion area shown. Graphs represent the mean ± SD, *P <0.05, **P < 0.01, ***P < 0.001, ****P < 0.0001 (n = 3).

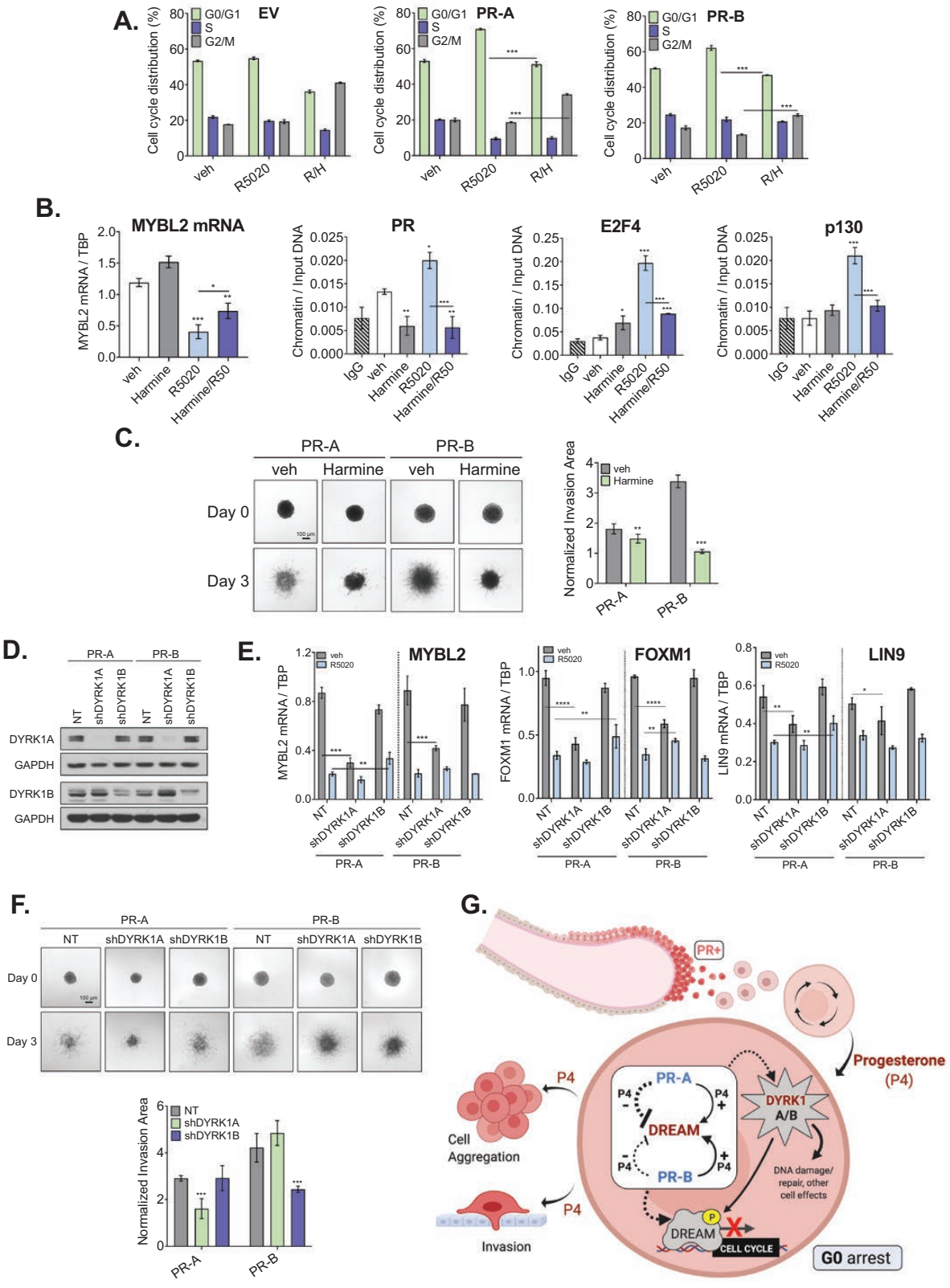

Figure 7. DYRK1 inhibition interferes with PR-driven cell phenotypes in hFTE models. **A,** Cell cycle analyses (FACS) of hFTE, vehicle (veh), R5020 (10nM) or R5020+harmine (R/H) for 24 hours. **B,** Gene regulation in absence/presence of harmine: *Left:* regulation of MYBL2 mRNA vehicle (veh), harmine (10μM), R5020 (10nM) or R5020+harmine (R/H) for 72 hours. *Right 3 graphs:* ChIP assays of PR, p130 and E2F4 recruitment to the E2F4 binding site within the MYBL2 promoter (site #2), following 3-hour treatment with vehicle, harmine (30 minutes pretreatment; 10μM), R5020 (10nM)

the MYBL2 gene by interfering with the recruitment of DREAM complex members (E2F4, p130) and PR-B to these genes (Fig. 7B).

Additionally, harmine treatment included during primary spheroid formation led to a slight decrease in spheroid diameter (Supplemental Fig. 9A (32)) whereas reaggregated spheroid cultures resulted in no viable spheroids observed in harmine alone for both isoforms or for combined harmine and R5020 treatment in the PR-A+ hFTE (Supplemental Fig. 9B (32)). A significant reduction in spheroid diameter was also observed in harmine-treated PR-B+ hFTE. Interestingly, spheroid formation in the presence of R5020 followed by encasement in collagen I matrix for 72 hours, in the absence (vehicle) or presence of harmine, resulted in an almost complete blockage of collagen invasion, especially for highly invasive PR-B+ cells (Fig. 7C).

To implicate a specific DYRK1 isoform(s) in PR regulation of DREAM, knockdown of either DYRK1A or DYRK1B was performed in PR+ hFTE lines and subsequent analyses of PR-induced gene regulation and cancer-associated cell phenotypes were repeated. The mRNA and protein expression of each kinase (DYRK1A or DYRK1B) was depleted singly in each cell line (Fig. 7D; Supplemental Fig. 10A (32)). As with harmine, DYRK knockdown altered transcriptional regulation of DREAM-relevant genes. A strong attenuation of the basal (vehicle) expression of MYBL2, LIN9, and FOXM1 was observed in both PR-A+ and PR-B+ hFTE in the DYRK1A-depleted state (Fig. 7E). In the presence of progestin (R5020 treated), we previously observed that both PR isoforms strongly repress the expression of these genes (see Supplemental Fig. 7B (32)) as observed in the nontargeting control (NT). This may indicate that progestin regulation of these genes is lost or nonresponsive due to the lower basal levels of these genes in the DYRK1A-depleted state. DYRK1B-depleted PR-A+ hFTE treated with R5020 showed an attenuation of this repression, exhibiting greater relative expression levels as compared with control NT cells treated with R5020 (Fig. 7E). Similarly treated, DYRK1B-depleted PR-B+ hFTE showed no significant change. More importantly, depletion of DYRK1A or DYRK1B also attenuated the PR-induced enhancement of cell aggregation and reaggregation in both PR-A+ and PR-B+ hFTE (Supplemental Fig. 10B and 10C (32)) with reaggregation showing the most robust effect. Interestingly, for some of the biological readouts, the effect of silencing each kinase was highly PR isoform-specific. In collagen invasion assays, for example, depletion of DYRK1A resulted in an almost total block of PR-A+ cell invasion whereas DYRK1B shRNA had no effect (Fig. 7F). In contrast, DYRK1B depletion reduced PR-B+ cell invasion; DYRK1A shRNA had no effect (Fig. 7F). These data support a novel role for DYRK1 isoforms as mediators of both PR-A (DYRK1A) and PR-B (DYRK1B) transcriptional responses and cancer cell-associated behaviors.

Taken together, the data presented here suggest a model wherein PR signaling promotes changes in hFTE cell fate that enable early stages of HGSC progression (Fig. 7G). In the absence of progestin, unliganded PR-A inhibits DREAM/DYRK1 actions, supporting permissive proliferation. In the presence of progestins, PRs mediate the transcriptional regulation of DREAM complex proteins and promote formation of active (ie, repressive) DREAM complexes that require p130 and DYRK1. Thus, liganded PRs support the DREAM/DYRK1-mediated repression of cell cycle-dependent genes and the subsequent arrest in G0. This quiescent state, along with other direct actions of PRs (ie, in part mediated via PR isoform specific use of DYRKs) may promote cell survival by supporting cell aggregation and spheroid formation following shedding from the fallopian tube. Once PR+ tumor emboli are circulating within the abdominal cavity, a hormone-rich microenvironment may promote their subsequent invasion of the mesothelial layer lining the peritoneal cavity. Further imbalance of DREAM or PR isoforms (ie, loss of p130 or PR) may permit cell cycle re-entry at distant sites.

Discussion

The actions of ovarian steroid hormones such as progesterone are known to be highly contextual and complex; they are dependent on the tissue, the specific cell type, as well as the local hormonal milieu. Within breast tissue, progesterone can be tumor-promoting or protective; its effects greatly influenced by the hormone concentration, the duration of exposure, presence of other steroids and signaling molecules, and the age of the woman (15, 73). In reproductive tract tissues such as the uterus, progesterone has traditionally been viewed as a protective factor due to its

Figure 7: continued

or harmine+R5020 in PR-B+ hFTE. **C,** Collagen invasion assay of hFTE spheroid cultures treated with R5020 (10nM; 72 hours), then embedded into collagen with vehicle (veh; DMSO) or harmine (10μM; 72 hours). **D,** DYRK1A and DYRK1B protein expression in the hFTE PR-A+ and PR-B+ NT, shDYRK1A and shDYRK1B cell models. GAPDH shown as loading control. **E,** Gene expression of DREAM and B-MYB/MMB complex proteins (LIN9, MYBL2, FOXM1) in NT, shDYRK1A and shDYRK1B PR-A and PR-B hFTE cell models. **F,** Collagen invasion assay of hFTE PR-A+ and PR-B+ NT, shDYRK1A and shDYRK1B spheroid cultures as indicated in Fig. 6F. **G,** Model depicting the actions of PR and progesterone in fallopian tube epithelia. Figure created with BioRender.com. Graphs represent the mean ± SD, $^{**}P < 0.01$, $^{***}P < 0.001$, $^{****}P < 0.0001$ (n = 3).

antagonistic actions on estrogen-induced endometrial proliferation (15). The work presented here shows another facet of progesterone's actions in the reproductive tract—this hormone, in the context of mutations within early fallopian tube lesions, may drive reversible cell cycle arrest and associated cell behaviors that could contribute to OC progression.

The functions of PR are intimately connected to cell fate and stemness. PR senses inputs from sex hormone and growth factor–initiated signals, integrating these with activation of multiple kinase pathways that ultimately modulate cell cycle progression (16, 74, 75). From studies conducted in breast, uterine, and ovarian carcinoma models, PR is known to be tightly coupled to cell cycle mediators via cell cycle dependent PR phosphorylation (76), direct PR-cyclin (D1, A, and E1), or PR- cyclin-dependent kinase (CDK2) interactions along with transcriptional regulation of critical cell cycle genes (76-78). The connection between PR actions and DREAM complex function revealed by our studies is a novel mechanism by which progesterone can manipulate cell fate—unique in the context of fallopian tube epithelia and previously unreported as a downstream effect of PR signaling. Studies in breast carcinoma lines have shown that the estrogen antagonist, ICI 182780, can induce an increase in p130 (*RBL2*) protein and p130/E2F4 complex accumulation (79). Progesterone was able to reduce phosphorylation of p107 (*RBL1*), inhibiting estrogen-induced proliferation in uterine epithelia (80) and synthetic progestins alone showed similar effect on p107 phosphorylation in T47D breast cancer cells (81). None of these studies connected the actions of either estrogen or progesterone or their receptors to direct modulation of DREAM complexes, at both the level of protein complex formation and transcriptional regulation of DREAM complex components as we have shown.

Multiple experimental approaches were utilized in our studies to interfere with DREAM complex, including E6/E7 immortalized cell line (ie, in which p130 is naturally depleted via degradation), chemotherapeutic blockade (harmine) of DYRK1 kinase function, and depletion (shRNA knockdown) of DYRK1A/1B kinase expression. These approaches consistently prevented the progestin-induced cell cycle arrest and totally abolished or attenuated the transcriptional regulation of genes encoding DREAM complex proteins and/or cell cycle dependent proteins known as DREAM targets. This suggests that progestins induce G0 cell cycle arrest, in part, through the modulation of DREAM function. The cell behaviors of cell-cell aggregation and collagen invasion exhibited more variable attenuation/abolishment upon DREAM interference, implying that the G0 state mediated by DREAM/DYRK1 kinases contributes to, but is not the sole regulator of, these PR/progestin-mediated phenotypes (ie, inhibition of proliferation was separable from other cancer-associated phenotypes in the E6/E7 immortalized cells). Therefore, direct effects of PR expression and progestins also drive these behaviors (cell aggregation/invasion) even when cell growth inhibition is disabled by loss of p130.

Progestins are known to regulate cell migration and invasion in advanced cancer models. In multiple breast cancer lines, PR signaling enhances migration and invasion through stabilization of the RhoA complex, modulation of focal adhesions, and transcriptional regulation of key genes (82-84). Progesterone, allopregnanolone, and mifepristone (RU486) have been shown to increase migration in ovarian carcinoma lines (85, 86). Pathway analyses of our PR+ hFTE showed that PR expression modulated genes associated with cell morphogenesis, cell-cell and cell-matrix adhesion, as well as Rho signaling (Supplemental Fig. 6B (32)). Studies have observed that p53 mutations can support enhanced cell adhesion and mesothelial invasion in immortalized "normal" hFTE cell lines (48). Though interplay between PR activation and wild-type p53 expression and their transcriptional effects has been reported (87, 88), an understanding of the mechanisms of this interaction and subsequent modulation of metastatic phenotypes is limited. It is interesting to note that recent work has revealed several p53 mutant species, including R175H, can disrupt the progesterone-activated PR-A/p53 complexes that regulate p27 expression, but no downstream phenotypic effects were explored (87). It remains to be proven if mutant p53 species in FTE can synergize with progestins to support these cell behaviors. Further research will be needed to determine how additional commonly observed genetic alterations in STICs, such as Cyclin E1 (CCNE1) amplification (47, 89), BRCA1/2 mutations (12), or viral (HPV) infection (90, 91) could further modify PR signaling. Notably, both cyclins/CDKs (76, 92) and BRCA1/2 (93) are known PR-binding proteins.

The ratio of PR isoforms in a cell, the presence of potential ligands, and posttranslational receptor modifications (ie, phosphorylation) all contribute to the downstream cellular outcomes of PR signaling (15-17). In our hFTE models, PR-A+ cells without progestins (ie, ligand-*independent*) were more proliferative and migratory, whereas PR-B+ cells with progestins (ie, ligand-*dependent*) were more invasive. Such distinct effects have been observed in other advanced cancer models and could modulate PR signaling in normal FTE as well as during the progression to early neoplasms. For example, PR-A actions drive stemness in breast carcinoma models while PR-B primarily promotes proliferation; opposite isoform effects compared with our hFTE models (94, 95). In addition, recent mouse models of

constitutive PR isoform overexpression have revealed that PR-B was the stronger driver of proliferation in the development and progression of ovarian neoplasms originating from ovarian luteal cells (78). In normal human and mouse fallopian tube, these isoforms appear to be equally expressed, but the question of whether changes (ie, imbalance) in isoform expression occur in early STIC lesions is currently unknown. IHC studies of PR isoform staining across advanced OC tumor subtypes would suggest a loss of PR-A protein expression during disease progression, opposite to the PR-A dominance (ie, loss of PR-B protein) observed in breast cancer (96-98). While PR isoform imbalance is a hallmark of hormone-driven cancers (15), it is possible that loss of PR isoform IHC epitopes, as commonly measured using clinical monoclonal antibodies, represents the presence of highly modified/activated receptors (18, 46). In addition, clinical-grade PR monoclonal antibodies may exhibit unequal detection of PR isoforms (99, 100). Therefore, the variability of PR protein expression previously reported in STICs (101) and invasive HGSC (102, 103) using such antibodies could be an artifact of the limitations of monoclonal antibodies and is most likely missing an important component of PR signaling, wherein p-PR is a biomarker of activated PR. The opposing actions of unliganded PR-A relative to liganded PR-B are likely highly context-dependent. Our data support a model whereby in FTE exposed to low/no progesterone (ie, postmenopausal or hormone-ablated contexts), PR-A may dominantly repress DREAM (PR-A+ hFTE cells proliferate freely), while in the presence of abundant progesterone, both PRs, but especially PR-B, may dominantly activate DREAM (PR+ hFTE cells exit the cell cycle). This relationship between PR isoforms perhaps ensures a decisive or "switch-like" and robust response to hormonal cycles. Notably, while STICs give rise to invasive serous OC, they appear to preexist for years to decades as relatively dormant (STIL) lesions. In light of our IHC analyses, activated (ie, phosphorylated) PRs may drive the enhancement of DREAM and thus maintain cellular quiescence in early lesions (ie, when progesterone is present). The decline of ovarian progesterone during peri/postmenopausal transitions, in addition to the accumulation of genetic alterations (discussed above), may "release" PR-mediated cell cycle blocks and instead enable proliferation, cell-cell aggregation, and invasion in PR+ cells in STILs thereby facilitating transition to STICs. Therefore, future IHC studies of phospho-PR species and quiescence markers in STILs/STICs and associated invasive lesions from a larger, more diverse cohort of both pre- and postmenopausal patients could help differentiate between the PR isoforms present and their signaling potential, clarifying the role of changing PR signaling as well as altered expression of DREAM components (ie, a release of PR-dependent repression) during HGSC progression.

The distinct isoform-specific effects of DYRK1A or DYRK1B kinase depletion in the unliganded and liganded PR-A+ vs PR-B+ hFTE were unexpected. For example, we observed that collagen invasion was abolished in PR-A+ hFTE only when DYRK1A was depleted whereas there was no effect of DYRK1B depletion. Interestingly, both PR-A+ and PR-B+ hFTE exhibited unique attenuation of basal gene expression in an unliganded state (vehicle) with DYRK1A depletion, potentially revealing a more prominent role of this kinase in unliganded PRs regulation of cell cycle dependent transcription. In contrast, DYRK1B depletion exposed a potential role of DYRK1B in liganded PR regulation, especially for PR-A, since loss of this kinase partially reversed the strong R5020-mediated repression normally seen in unaltered hFTE cells. No published studies have examined these kinases in the context of FTE and/or PR signaling. Both kinases can promote G0 arrest through DREAM and other mechanisms, and inhibition or depletion of either can induce cell cycle re-entry in normal and cancer cells (66, 69). But recent studies are expanding the function of these kinases, in particular, their role in DNA damage repair. DYRK1A is proposed to be involved in DNA double-stranded break repair by modulating 53BP1 recruitment, thereby supporting a shift to error-prone nonhomologous end joining repair pathways (49). This is intriguing, since preliminary studies in our laboratory suggest that the progestins enhance DNA damage (unpublished results). Therefore, it will be interesting to further explore the regulation and activity of DYRK1 kinases and the potential interplay between PR signaling and kinase actions in early lesions.

The evolution of HGSC makes a PR-driven quiescent state, and its potential to promote pro-survival/pro-dissemination phenotypes, highly relevant to our understanding of disease etiology. The presence of total and nuclear "focal" and phosphorylated PRs observed in STICs and invasive tumors revealed in our studies suggests that active PR signaling in these lesions could be promoting cell dormancy. Such promotion of dormancy by these activated PR could be perceived as protective—for example, minimizing the effects of cellular stressors that bathe the distal fimbriae of the fallopian tube (104). However, research in cancer, aging, and stem cell dynamics has revealed that quiescence comes at a cost. Slow-cycling/quiescent cells must rely on nonhomologous end joining, an error-prone mechanism for DNA damage repair that can lead to misrepaired double-stranded breaks, mutagenesis, and genomic instability (105). In addition, dormant cancer cells often display more aggressive migratory and invasive behaviors

(106, 107) and exhibit chemoresistance to therapeutics that target proliferating cells (29). Blocking DREAM formation and quiescence in advanced OC models, through depletion of DYRK1A, DYRK1B, or p130/RB2, leads to lack of spheroid formation, reduced viability, increased apoptosis, and sensitization to platin therapeutics (30, 72).

A quiescent cell can be stimulated to re-enter the cell cycle and, depending on the "health" of that cell (eg, DNA damage, levels of reactive oxygen species), go on to proliferate, enter senescence (which potentially can be reversible) or undergo regulated cell death (29). Previous work in our laboratory has revealed progestin-mediated, PR-A- and PR-B-dependent cellular senescence in advanced OC cell models (9). Other researchers have suggested that progesterone can cause apoptosis (108) or necroptosis (109); these studies often are complicated by high hormone treatment levels and lack of nuclear receptor expression. Taken together, it is probable that during OC progression, the effects of PR and progestins will be nuanced, depending on signaling inputs resulting from genetic alterations and microenvironment changes. Such shifts in PR actions have been observed in breast cancer, where progesterone will drive migration in early lesions, prior to a detectable tumor, yet promote proliferation during metastasis (110). In addition, the ligand-independent effects that our studies have revealed suggests that although certain physiological states exhibit low or no progesterone (ie, postmenopausal), this should not negate the capacity of these receptors to drive cellular outcomes in early and advanced stages of HGSC. The studies presented here provide evidence for a novel mechanism of PR signaling in healthy fallopian tube epithelia as well as those in a compromised state that could lead to disease initiation and progression. For example, in HPV-infected FTE, the cell cycle would be predicted to be "released" from progesterone blockade, while other PR-driven cancer phenotypes (cell aggregation/invasion) are robustly promoted.

Our findings represent an alternative perspective on the idea that progesterone always confers protection against ovarian cancers. In our studies, PRs support a quiescent FTE cell fate through modulation of DREAM/DYRK1 function and such a state could be protective. But, over an extended period, quiescence can also be associated with many of the hallmarks of cancer such as the acquisition of new mutations, the survival in a suboptimal environment, metastasis, and chemoresistance (28, 29). In addition, the potential for coincident dysregulation of DREAM components in FTE, an event often observed in cancers (27, 31), along with the emerging role of DYRK1 kinases in DNA damage repair (111), the cellular outcomes of PR signaling will be nuanced and highly contextual, like other sex steroids. This idea that PR signaling could promote cellular states that enhance ovarian cancer risk is supported by recently published research showing progesterone-driven ovarian tumor progression in transgenic mouse models (78). Taken together, we might consider an expanded view of another role of progesterone/PR as contributing factors in the development of STICs that progress to HGSC. Considering that occult STICs can reside undetected within FT for decades prior to established invasive disease, there are now significant clinical opportunities to prevent the ultimate development of HGSC by targeting PRs, DREAM, and/or DYRKs (ie, as with harmine). Since existing antiprogestins (onapristone, RU486) behave as PR agonists in hFTE (Supplemental Fig. 4 (32)), we suggest that trials of clinical interventions directly targeting PRs as a means to eliminate STICs in high-risk women proceed with caution until more effective (ie, pure antagonists or PR degraders) are developed.

Acknowledgments

The authors thank members of the Lange and Ostrander laboratories for technical and intellectual contributions; Dr. K. Schwertfeger for editorial comments; Mei Zhang for histological processing and staining; Dr. J. Burdette for kindly providing mouse oviductal epithelial cell lines; Intelligene Technologies for bioinformatics services using the Artificial Intelligene platform; the staff of the Clinical & Translational Science Institute (CTSI) Biorepository and Laboratory Services for tissue collection; and the University Imaging Center (UIC) for microscopy and slide scanning services. The CTSI program is supported by the National Institutes of Health's Clinical and Translational Science Award (UL1TR002494).

Financial Support: Minnesota Ovarian Cancer Alliance (CAL, LJM), University of Minnesota Office of the VP for Research (LJM, CAL), National Institutes of Health R01CA229697 (CAL), National Institutes of Health R01CA188571 (LL), National Cancer Institute SPORE Ovarian cancer P50 CA228991 (RD), Dr. Miriam and Sheldon G. Adelson Medical Research Foundation (RD), and Claneil Foundation (RD).

Author Contributions: Conception and design, L.J. Mauro, C.A. Lange; development of methodology, L.J. Mauro, M. Seibel, A. Spartz, C. Diep, L. Litovchick, E.M. Swisher, H. Singhal; acquisition of data, M. Seibel, C. Diep, A. Spartz, S. Saini, F. Sesay, L.E. Schwartz, L.J. Mauro; analysis and interpretation of data, M. Seibel, A. Spartz, C. Diep, L. Litovchick, S. Saini, F. Sesay, C. Perez Kerkvliet, L.E. Schwartz, R. Drapkin, H. Singhal, L.J. Mauro, C.A. Lange; writing, review and/or revision of manuscript, M. Seibel, C. Diep, L. Litovchick, R. Drapkin, H. Singhal, L.J. Mauro, C.A. Lange.

Additional Information

Current Affiliation: Siddharth Saini's current affiliation is Department of Biochemistry & Molecular Pharmacology, NYU Grossman School of Medicine, NY, NY 10016.

Correspondence: L. J. Mauro, PhD, University of Minnesota, 495F AnSc/VM Bldg, 1988 Fitch Ave, Saint Paul, MN 55108, USA. Email: mauro002@umn.edu; or C. A. Lange, PhD, University of Minnesota, CCRB Mail Delivery Code 2812A, 2231 6th St SE, Minneapolis, MN 55455, USA. Email: lange047@umn.edu.

Disclosure: C. A. Lange is a consultant/scientific advisory board member for Context Therapeutics, Inc. H. Singhal is an employee of Hoffmann-La Roche. R. Drapkin is a consultant/advisory board member for Repare Therapeutics, Mersana Therapeutics, and Siamab Therapeutics.

Data Availability: Some or all data generated or analyzed during this study are included in this published article or in the data repositories listed in the References. RNAseq data collected in these studies has been deposited in NCBI Gene Expression Omnibus (GEO) database (41). Supplemental figures are available at Figshare digital repository (32).

References

1. Cronin KA, Lake AJ, Scott S, et al. Annual Report to the Nation on the Status of Cancer, part I: National cancer statistics. *Cancer*. 2018;**124**(13):2785-2800.
2. Reid BM, Permuth JB, Sellers TA. Epidemiology of ovarian cancer: a review. *Cancer Biol Med*. 2017;**14**(1):9-32.
3. Bešević J, Gunter MJ, Fortner RT, et al. Reproductive factors and epithelial ovarian cancer survival in the EPIC cohort study. *Br J Cancer*. 2015;**113**(11):1622-1631.
4. Iversen L, Fielding S, Lidegaard Ø, Mørch LS, Skovlund CW, Hannaford PC. Association between contemporary hormonal contraception and ovarian cancer in women of reproductive age in Denmark: prospective, nationwide cohort study. *Bmj*. 2018;**362**:k3609.
5. Wentzensen N, Poole EM, Trabert B, et al. Ovarian Cancer Risk Factors by Histologic Subtype: An Analysis From the Ovarian Cancer Cohort Consortium. *J Clin Oncol*. 2016;**34**(24):2888-2898.
6. Collaborative Group On Epidemiological Studies Of Ovarian C, Beral V, Gaitskell K, Hermon C, Moser K, Reeves G, Peto R. Menopausal hormone use and ovarian cancer risk: Individual participant meta-analysis of 52 epidemiological studies. *Lancet*. 2015;**385**(9980):1835-1842.
7. Beral V, Bull D, Green J, Reeves G; Million Women Study Collaborators. Ovarian cancer and hormone replacement therapy in the Million Women Study. *Lancet*. 2007;**369**(9574):1703-1710.
8. Diep CH, Charles NJ, Gilks CB, Kalloger SE, Argenta PA, Lange CA. Progesterone receptors induce FOXO1-dependent senescence in ovarian cancer cells. *Cell Cycle*. 2013;**12**(9):1433-1449.
9. Diep CH, Knutson TP, Lange CA. Active FOXO1 Is a Key Determinant of Isoform-Specific Progesterone Receptor Transactivation and Senescence Programming. *Mol Cancer Res*. 2016;**14**(2):141-162.
10. Liu JF, Hirsch MS, Lee H, Matulonis UA. Prognosis and hormone receptor status in older and younger patients with advanced-stage papillary serous ovarian carcinoma. *Gynecol Oncol*. 2009;**115**(3):401-406.
11. Lee Y, Miron A, Drapkin R, et al. A candidate precursor to serous carcinoma that originates in the distal fallopian tube. *J Pathol*. 2007;**211**(1):26-35.
12. Labidi-Galy SI, Papp E, Hallberg D, et al. High grade serous ovarian carcinomas originate in the fallopian tube. *Nat Commun*. 2017;**8**(1):1093.
13. Ducie J, Dao F, Considine M, et al. Molecular analysis of high-grade serous ovarian carcinoma with and without associated serous tubal intra-epithelial carcinoma. *Nat Commun*. 2017;**8**(1):990.
14. Wu RC, Wang P, Lin SF, et al. Genomic landscape and evolutionary trajectories of ovarian cancer precursor lesions. *J Pathol*. 2019;**248**(1):41-50.
15. Diep CH, Daniel AR, Mauro LJ, Knutson TP, Lange CA. Progesterone action in breast, uterine, and ovarian cancers. *J Mol Endocrinol*. 2015;**54**(2):R31-R53.
16. Pierson-Mullany LK, Skildum A, Faivre E, Lange CA. Cross-talk between growth factor and progesterone receptor signaling pathways: implications for breast cancer cell growth. *Breast Dis*. 2003;**18**:21-31.
17. Daniel AR, Lange CA. Protein kinases mediate ligand-independent derepression of sumoylated progesterone receptors in breast cancer cells. *Proc Natl Acad Sci U S A*. 2009;**106**(34):14287-14292.
18. Knutson TP, Daniel AR, Fan D, et al. Phosphorylated and sumoylation-deficient progesterone receptors drive proliferative gene signatures during breast cancer progression. *Breast Cancer Res*. 2012;**14**(3):R95.
19. Knutson TP, Truong TH, Ma S, et al. Posttranslationally modified progesterone receptors direct ligand-specific expression of breast cancer stem cell-associated gene programs. *J Hematol Oncol*. 2017;**10**(1):89.
20. Daniel AR, Knutson TP, Lange CA. Signaling inputs to progesterone receptor gene regulation and promoter selectivity. *Mol Cell Endocrinol*. 2009;**308**(1-2):47-52.
21. Daniel AR, Gaviglio AL, Knutson TP, et al. Progesterone receptor-B enhances estrogen responsiveness of breast cancer cells via scaffolding PELP1- and estrogen receptor-containing transcription complexes. *Oncogene*. 2015;**34**(4):506-515.
22. Cvoro A, Tzagarakis-Foster C, Tatomer D, Paruthiyil S, Fox MS, Leitman DC. Distinct roles of unliganded and liganded estrogen receptors in transcriptional repression. *Mol Cell*. 2006;**21**(4):555-564.
23. Dressing GE, Lange CA. Integrated actions of progesterone receptor and cell cycle machinery regulate breast cancer cell proliferation. *Steroids*. 2009;**74**(7):573-576.
24. Li S, Winuthayanon W. Oviduct: roles in fertilization and early embryo development. *J Endocrinol*. 2017;**232**(1):R1-R26.
25. Eddie SL, Quartuccio SM, Zhu J, et al. Three-dimensional modeling of the human fallopian tube fimbriae. *Gynecol Oncol*. 2015;**136**(2):348-354.
26. Lawrenson K, Notaridou M, Lee N, et al. In vitro three-dimensional modeling of fallopian tube secretory epithelial cells. *BMC Cell Biol*. 2013;**14**:43.
27. Iness AN, Litovchick L. MuvB: A Key to Cell Cycle Control in Ovarian Cancer. *Front Oncol*. 2018;**8**:223.
28. Sosa MS, Bragado P, Aguirre-Ghiso JA. Mechanisms of disseminated cancer cell dormancy: an awakening field. *Nat Rev Cancer*. 2014;**14**(9):611-622.
29. Recasens A, Munoz L. Targeting Cancer Cell Dormancy. *Trends Pharmacol Sci*. 2019;**40**(2):128-141.
30. Hu J, Nakhla H, Friedman E. Transient arrest in a quiescent state allows ovarian cancer cells to survive suboptimal growth

conditions and is mediated by both Mirk/dyrk1b and p130/RB2. *Int J Cancer*. 2011;**129**(2):307-318.
31. Iness AN, Felthousen J, Ananthapadmanabhan V, et al. The cell cycle regulatory DREAM complex is disrupted by high expression of oncogenic B-Myb. *Oncogene*. 2019;**38**(7):1080-1092.
32. Mauro LJ, Seibel MI, Diep CH, et al. Data from: Progesterone receptors promote quiescence and ovarian cancer cell phenotypes via regulation of dream in p53-mutant fallopian tube models. *figshare*. Posted February 15, 2021. https://doi.org/10.6084/m9.figshare.14035958
33. Yemelyanova A, Vang R, Kshirsagar M, et al. Immunohistochemical staining patterns of p53 can serve as a surrogate marker for TP53 mutations in ovarian carcinoma: an immunohistochemical and nucleotide sequencing analysis. *Mod Pathol*. 2011;**24**(9):1248-1253.
34. Dean M, Jin V, Bergsten TM, et al. Loss of PTEN in fallopian tube epithelium results in multicellular tumor spheroid formation and metastasis to the ovary. *Cancers (Basel)*. 2019;**11**(6):884.
35. Halbert CL, Demers GW, Galloway DA. The E6 and E7 genes of human papillomavirus type 6 have weak immortalizing activity in human epithelial cells. *J Virol*. 1992;**66**(4):2125-2134.
36. Dobin A, Davis CA, Schlesinger F, et al. STAR: ultrafast universal RNA-seq aligner. *Bioinformatics*. 2013;**29**(1):15-21.
37. Trapnell C, Roberts A, Goff L, et al. Differential gene and transcript expression analysis of RNA-seq experiments with TopHat and Cufflinks. *Nat Protoc*. 2012;**7**(3):562-578.
38. Love MI, Huber W, Anders S. Moderated estimation of fold change and dispersion for rna-seq data with deseq2. *Genome Biol*. 2014;**15**(12):550.
39. Subramanian A, Tamayo P, Mootha VK, et al. Gene set enrichment analysis: a knowledge-based approach for interpreting genome-wide expression profiles. *Proc Natl Acad Sci U S A*. 2005;**102**(43):15545-15550.
40. Lee O, Sullivan ME, Xu Y, et al. Selective Progesterone Receptor Modulators in Early-Stage Breast Cancer: A Randomized, Placebo-Controlled Phase II Window-of-Opportunity Trial Using Telapristone Acetate. *Clin Cancer Res*. 2020;**26**(1):25-34.
41. Mauro LJ, Seibel MI, Diep CH, et al. Data from: Progesterone receptors promote quiescence and ovarian cancer cell phenotypes via regulation of dream in p53-mutant fallopian tube models. Gene expression Omnibus (GEO) database. Deposited October 12, 2020; updated March 31, 2021. https://www.ncbi.nlm.nih.gov/geo/query/acc.cgi?acc=GSE126775
42. Kim KH, Sederstrom JM. Assaying Cell Cycle Status Using Flow Cytometry. *Curr Protoc Mol Biol*. 2015;**111**:28.6.1-28.6.11.
43. Arnett-Mansfield RL, Graham JD, Hanson AR, et al. Focal subnuclear distribution of progesterone receptor is ligand dependent and associated with transcriptional activity. *Mol Endocrinol*. 2007;**21**(1):14-29.
44. Bonneterre J, Hutt E, Bosq J, et al. Development of a technique to detect the activated form of the progesterone receptor and correlation with clinical and histopathological characteristics of endometrioid adenocarcinoma of the uterine corpus. *Gynecol Oncol*. 2015;**138**(3):663-667.
45. Daniel AR, Faivre EJ, Lange CA. Phosphorylation-dependent antagonism of sumoylation derepresses progesterone receptor action in breast cancer cells. *Mol Endocrinol*. 2007;**21**(12):2890-2906.
46. Lange CA, Shen T, Horwitz KB. Phosphorylation of human progesterone receptors at serine-294 by mitogen-activated protein kinase signals their degradation by the 26S proteasome. *Proc Natl Acad Sci U S A*. 2000;**97**(3):1032-1037.
47. Karst AM, Jones PM, Vena N, et al. Cyclin E1 deregulation occurs early in secretory cell transformation to promote formation of fallopian tube-derived high-grade serous ovarian cancers. *Cancer Res*. 2014;**74**(4):1141-1152.
48. Iwanicki MP, Chen HY, Iavarone C, et al. Mutant p53 regulates ovarian cancer transformed phenotypes through autocrine matrix deposition. *JCI Insight*. 2016;**1**(10).e86829.
49. Shield K, Ackland ML, Ahmed N, Rice GE. Multicellular spheroids in ovarian cancer metastases: Biology and pathology. *Gynecol Oncol*. 2009;**113**(1):143-148.
50. Burleson KM, Boente MP, Pambuccian SE, Skubitz AP. Disaggregation and invasion of ovarian carcinoma ascites spheroids. *J Transl Med*. 2006;**4**:6.
51. Beck CA, Weigel NL, Moyer ML, Nordeen SK, Edwards DP. The progesterone antagonist RU486 acquires agonist activity upon stimulation of cAMP signaling pathways. *Proc Natl Acad Sci U S A*. 1993;**90**(10):4441-4445.
52. Smith CL, O'Malley BW. Coregulator function: a key to understanding tissue specificity of selective receptor modulators. *Endocr Rev*. 2004;**25**(1):45-71.
53. Hammes SR, Levin ER. Minireview: Recent advances in extranuclear steroid receptor actions. *Endocrinology*. 2011;**152**(12):4489-4495.
54. Thomas P. Characteristics of membrane progestin receptor alpha (mPRalpha) and progesterone membrane receptor component 1 (PGMRC1) and their roles in mediating rapid progestin actions. *Front Neuroendocrinol*. 2008;**29**(2):292-312.
55. Iwanicki MP, Davidowitz RA, Ng MR, et al. Ovarian cancer spheroids use myosin-generated force to clear the mesothelium. *Cancer Discov*. 2011;**1**(2):144-157.
56. Kenny HA, Nieman KM, Mitra AK, Lengyel E. The first line of intra-abdominal metastatic attack: breaching the mesothelial cell layer. *Cancer Discov*. 2011;**1**(2):100-102.
57. Shield K, Riley C, Quinn MA, Rice GE, Ackland ML, Ahmed N. Alpha2beta1 integrin affects metastatic potential of ovarian carcinoma spheroids by supporting disaggregation and proteolysis. *J Carcinog*. 2007;**6**:11.
58. Jacobsen BM, Richer JK, Sartorius CA, Horwitz KB. Expression profiling of human breast cancers and gene regulation by progesterone receptors. *J Mammary Gland Biol Neoplasia*. 2003;**8**(3):257-268.
59. Drapkin R, von Horsten HH, Lin Y, et al. Human epididymis protein 4 (HE4) is a secreted glycoprotein that is overexpressed by serous and endometrioid ovarian carcinomas. *Cancer Res*. 2005;**65**(6):2162-2169.
60. Tempest N, Baker AM, Wright NA, Hapangama DK. Does human endometrial LGR5 gene expression suggest the existence of another hormonally regulated epithelial stem cell niche? *Hum Reprod*. 2018;**33**(6):1052-1062.
61. Chang YH, Ding DC, Chu TY. Estradiol and Progesterone Induced Differentiation and Increased Stemness Gene Expression of Human Fallopian Tube Epithelial Cells. *J Cancer*. 2019;**10**(13):3028-3036.
62. King AE, Morgan K, Sallenave JM, Kelly RW. Differential regulation of secretory leukocyte protease inhibitor and elafin by progesterone. *Biochem Biophys Res Commun*. 2003;**310**(2):594-599.

63. Fischer M, Grossmann P, Padi M, DeCaprio JA. Integration of TP53, DREAM, MMB-FOXM1 and RB-E2F target gene analyses identifies cell cycle gene regulatory networks. *Nucleic Acids Res*. 2016;**44**(13):6070-6086.
64. DeCaprio JA. Human papillomavirus type 16 E7 perturbs DREAM to promote cellular proliferation and mitotic gene expression. *Oncogene*. 2014;**33**(31):4036-4038.
65. Fischer M, Uxa S, Stanko C, Magin TM, Engeland K. Human papilloma virus E7 oncoprotein abrogates the p53-p21-DREAM pathway. *Sci Rep*. 2017;**7**(1):2603.
66. Becker W. A wake-up call to quiescent cancer cells - potential use of DYRK1B inhibitors in cancer therapy. *Febs J*. 2018;**285**(7):1203-1211.
67. DeCaprio JA, Duensing A. The DREAM complex in antitumor activity of imatinib mesylate in gastrointestinal stromal tumors. *Curr Opin Oncol*. 2014;**26**(4):415-421.
68. Soppa U, Becker W. DYRK protein kinases. *Curr Biol*. 2015;**25**(12):R488-R489.
69. Litovchick L, Florens LA, Swanson SK, Washburn MP, DeCaprio JA. DYRK1A protein kinase promotes quiescence and senescence through DREAM complex assembly. *Genes Dev*. 2011;**25**(8):801-813.
70. Hu J, Friedman E. Depleting Mirk Kinase Increases Cisplatin Toxicity in Ovarian Cancer Cells. *Genes Cancer*. 2010;**1**(8):803-811.
71. Ogawa Y, Nonaka Y, Goto T, et al. Development of a novel selective inhibitor of the Down syndrome-related kinase Dyrk1A. *Nat Commun*. 2010;**1**:86.
72. MacDonald J, Ramos-Valdes Y, Perampalam P, Litovchick L, DiMattia GE, Dick FA. A Systematic Analysis of Negative Growth Control Implicates the DREAM Complex in Cancer Cell Dormancy. *Mol Cancer Res*. 2017;**15**(4):371-381.
73. Brisken C, Hess K, Jeitziner R. Progesterone and Overlooked Endocrine Pathways in Breast Cancer Pathogenesis. *Endocrinology*. 2015;**156**(10):3442-3450.
74. Skildum A, Faivre E, Lange CA. Progesterone receptors induce cell cycle progression via activation of mitogen-activated protein kinases. *Mol Endocrinol*. 2005;**19**(2):327-339.
75. Daniel AR, Qiu M, Faivre EJ, Ostrander JH, Skildum A, Lange CA. Linkage of progestin and epidermal growth factor signaling: phosphorylation of progesterone receptors mediates transcriptional hypersensitivity and increased ligand-independent breast cancer cell growth. *Steroids*. 2007;**72**(2):188-201.
76. Dressing GE, Knutson TP, Schiewer MJ, et al. Progesterone receptor-cyclin D1 complexes induce cell cycle-dependent transcriptional programs in breast cancer cells. *Mol Endocrinol*. 2014;**28**(4):442-457.
77. Faivre EJ, Lange CA. Progesterone receptors upregulate Wnt-1 to induce epidermal growth factor receptor transactivation and c-Src-dependent sustained activation of Erk1/2 mitogen-activated protein kinase in breast cancer cells. *Mol Cell Biol*. 2007;**27**(2):466-480.
78. Wetendorf M, Li R, Wu S, et al. Constitutive expression of progesterone receptor isoforms promotes the development of hormone-dependent ovarian neoplasms. *Sci Signal*. 2020;**13**(652).eaaz9646.
79. Carroll JS, Prall OW, Musgrove EA, Sutherland RL. A pure estrogen antagonist inhibits cyclin E-Cdk2 activity in MCF-7 breast cancer cells and induces accumulation of p130-E2F4 complexes characteristic of quiescence. *J Biol Chem*. 2000;**275**(49):38221-38229.
80. Tong W, Pollard JW. Progesterone inhibits estrogen-induced cyclin D1 and cdk4 nuclear translocation, cyclin E- and cyclin A-cdk2 kinase activation, and cell proliferation in uterine epithelial cells in mice. *Mol Cell Biol*. 1999;**19**(3):2251-2264.
81. Musgrove EA, Swarbrick A, Lee CS, Cornish AL, Sutherland RL. Mechanisms of cyclin-dependent kinase inactivation by progestins. *Mol Cell Biol*. 1998;**18**(4):1812-1825.
82. Diaz J, Aranda E, Henriquez S, et al. Progesterone promotes focal adhesion formation and migration in breast cancer cells through induction of protease-activated receptor-1. *J Endocrinol*. 2012;**214**(2):165-175.
83. Bellance C, Khan JA, Meduri G, Guiochon-Mantel A, Lombès M, Loosfelt H. Progesterone receptor isoforms PRA and PRB differentially contribute to breast cancer cell migration through interaction with focal adhesion kinase complexes. *Mol Biol Cell*. 2013;**24**(9):1363-1374.
84. Fu XD, Goglia L, Sanchez AM, et al. Progesterone receptor enhances breast cancer cell motility and invasion via extranuclear activation of focal adhesion kinase. *Endocr Relat Cancer*. 2010;**17**(2):431-443.
85. Ponikwicka-Tyszko D, Chrusciel M, Stelmaszewska J, et al. Molecular mechanisms underlying mifepristone's agonistic action on ovarian cancer progression. *Ebiomedicine*. 2019;**47**:170-183.
86. Pelegrina LT, de Los Ángeles Sanhueza M, Ramona Cáceres AR, Cuello-Carrión D, Rodriguez CE, Laconi MR. Effect of progesterone and first evidence about allopregnanolone action on the progression of epithelial human ovarian cancer cell lines. *J Steroid Biochem Mol Biol*. 2020;**196**:105492.
87. Hsu SP, Lin PH, Chou CM, Lee WS. Progesterone up-regulates p27 through an increased binding of the progesterone receptor-A-p53 protein complex onto the non-canonical p53 binding motif in HUVEC. *J Steroid Biochem Mol Biol*. 2019;**185**:163-171.
88. Hsu SP, Yang HC, Kuo CT, et al. Progesterone receptor-NFκB complex formation is required for progesterone-induced NFκB nuclear translocation and binding onto the p53 promoter. *Endocrinology*. 2015;**156**(1):291-300.
89. Au-Yeung G, Lang F, Azar WJ, et al. Selective Targeting of Cyclin E1-Amplified High-Grade Serous Ovarian Cancer by Cyclin-Dependent Kinase 2 and AKT Inhibition. *Clin Cancer Res*. 2017;**23**(7):1862-1874.
90. Rosa MI, Silva GD, de Azedo Simões PW, et al. The prevalence of human papillomavirus in ovarian cancer: a systematic review. *Int J Gynecol Cancer*. 2013;**23**(3):437-441.
91. Kisseljova N, Zhordania K, Fedorova M, et al. Detection of Human Papillomavirus Prevalence in Ovarian Cancer by Different Test Systems. *Intervirology*. 2019;**62**(5-6):198-204.
92. Faivre E, Skildum A, Pierson-Mullany L, Lange CA. Integration of progesterone receptor mediated rapid signaling and nuclear actions in breast cancer cell models: role of mitogen-activated protein kinases and cell cycle regulators. *Steroids*. 2005;**70**(5-7):418-426.
93. Singhal H, Greene ME, Tarulli G, et al. Genomic agonism and phenotypic antagonism between estrogen and progesterone receptors in breast cancer. *Sci Adv*. 2016;**2**(6):e1501924.
94. Finlay-Schultz J, Cittelly DM, Hendricks P, et al. Progesterone downregulation of miR-141 contributes to expansion of

stem-like breast cancer cells through maintenance of progesterone receptor and Stat5a. *Oncogene*. 2015;**34**(28):3676-3687.
95. Finlay-Schultz J, Sartorius CA. Steroid hormones, steroid receptors, and breast cancer stem cells. *J Mammary Gland Biol Neoplasia*. 2015;**20**(1-2):39-50.
96. Akahira J, Inoue T, Suzuki T, et al. Progesterone receptor isoforms A and B in human epithelial ovarian carcinoma: immunohistochemical and RT-PCR studies. *Br J Cancer*. 2000;**83**(11):1488-1494.
97. Akahira J, Suzuki T, Ito K, et al. Differential expression of progesterone receptor isoforms A and B in the normal ovary, and in benign, borderline, and malignant ovarian tumors. *Jpn J Cancer Res*. 2002;**93**(7):807-815.
98. Lenhard M, Tereza L, Heublein S, et al. Steroid hormone receptor expression in ovarian cancer: progesterone receptor B as prognostic marker for patient survival. *BMC Cancer*. 2012;**12**:553.
99. Mote PA, Johnston JF, Manninen T, Tuohimaa P, Clarke CL. Detection of progesterone receptor forms A and B by immunohistochemical analysis. *J Clin Pathol*. 2001;**54**(8):624-630.
100. Fabris V, Abascal MF, Giulianelli S, et al. Isoform specificity of progesterone receptor antibodies. *J Pathol Clin Res*. 2017;**3**(4):227-233.
101. Nafisi H, Ghorab Z, Ismill N, et al. Immunophenotypic Analysis in Early Müllerian Serous Carcinogenesis. *Int J Gynecol Pathol*. 2015;**34**(5):424-436.
102. Sieh W, Köbel M, Longacre TA, et al. Hormone-receptor expression and ovarian cancer survival: an Ovarian Tumor Tissue Analysis consortium study. *Lancet Oncol*. 2013;**14**(9):853-862.
103. Tone AA, Virtanen C, Shaw PA, Brown TJ. Decreased progesterone receptor isoform expression in luteal phase fallopian tube epithelium and high-grade serous carcinoma. *Endocr Relat Cancer*. 2011;**18**(2):221-234.
104. King SM, Hilliard TS, Wu LY, Jaffe RC, Fazleabas AT, Burdette JE. The impact of ovulation on fallopian tube epithelial cells: evaluating three hypotheses connecting ovulation and serous ovarian cancer. *Endocr Relat Cancer*. 2011;**18**(5):627-642.
105. Mohrin M, Bourke E, Alexander D, et al. Hematopoietic stem cell quiescence promotes error-prone DNA repair and mutagenesis. *Cell Stem Cell*. 2010;**7**(2):174-185.
106. Kai F, Drain AP, Weaver VM. The Extracellular Matrix Modulates the Metastatic Journey. *Dev Cell*. 2019;**49**(3):332-346.
107. Gao XL, Zheng M, Wang HF, et al. NR2F1 contributes to cancer cell dormancy, invasion and metastasis of salivary adenoid cystic carcinoma by activating CXCL12/CXCR4 pathway. *BMC Cancer*. 2019;**19**(1):743.
108. Syed V, Ho SM. Progesterone-induced apoptosis in immortalized normal and malignant human ovarian surface epithelial cells involves enhanced expression of FasL. *Oncogene*. 2003;**22**(44):6883-6890.
109. Wu NY, Huang HS, Chao TH, et al. Progesterone Prevents High-Grade Serous Ovarian Cancer by Inducing Necroptosis of p53-Defective Fallopian Tube Epithelial Cells. *Cell Rep*. 2017;**18**(11):2557-2565.
110. Hosseini H, Obradović MMS, Hoffmann M, et al. Early dissemination seeds metastasis in breast cancer. *Nature*. 2016;**540**(7634):552-558.
111. Menon VR, Ananthapadmanabhan V, Swanson S, et al. DYRK1A regulates the recruitment of 53BP1 to the sites of DNA damage in part through interaction with RNF169. *Cell Cycle*. 2019;**18**(5):531-551.